Calculation of Exposure Profiles and Sensitivities of Options under the Heston and the Heston Hull-White Models

Q. Feng and C.W. Oosterlee

Abstract Credit Valuation Adjustment (CVA) has become an important field as its calculation is required in Basel III, issued in 2010, in the wake of the credit crisis. *Exposure*, which is defined as the potential future loss on a financial contract due to a default event, is one of the key elements for calculating CVA. This paper provides a backward dynamics framework for assessing exposure profiles of European, Bermudan and barrier options under the Heston and Heston Hull-White asset dynamics. We discuss the potential of the *Stochastic Grid Bundling Method* (SGBM), which is based on the techniques of *simulation*, *regression* and *bundling* (Jain and Oosterlee, Applied Mathematics and Computation, 269:412–431, 2015). By SGBM we can relatively easily compute the Potential Future Exposure (PFE) and sensitivities over the whole time horizon. Assuming independence between the default event and exposure profiles, we give here examples of calculating exposure, CVA and sensitivities for Bermudan and barrier options.

1 Introduction

In the wake of the credit crisis, regulators put more strict capital requirements to cover losses caused by default events. A recent capital charge was introduced in Basel III, i.e. the Credit Value Adjustment (CVA). CVA is the difference between the risk-free contract value and the contract value that accounts the possibility of a counterparty's default [16]. It can be computed as the integral over the time horizon as the expectation of the discounted losses on a default event, multiplied by the probability of default at that moment and the percentage of loss given default [30]. The computational complexity of CVA arises from the uncertainties of the losses

Q. Feng (✉)
Center for Mathematics and Computer Science (CWI), Amsterdam, The Netherlands
e-mail: qian@cwi.nl

C.W. Oosterlee
CWI and Delft University of Technology, Delft, The Netherlands
e-mail: c.w.oosterlee@cwi.nl

R. Melnik et al. (eds.), *Recent Progress and Modern Challenges in Applied Mathematics, Modeling and Computational Science*, Fields Institute Communications 79, DOI 10.1007/978-1-4939-6969-2_9

of a default event and the likelihood of the counterparty's default in the future. An unstable dependence structure between the counterparty's default probability and the corresponding losses in the future may exist, which makes the computation of CVA complicated [5, 16].

Credit *exposure* is defined as potential future losses without any recovery. Exposure evolves over time as the market moves with volatility, and typically cannot be expressed in closed form. Before the appearance in Basel II [2], concepts as expected exposure (EE) and potential future exposure (PFE) had emerged and were commonly used as the representative metrics for credit exposure [16]. EE represents the *average* expected loss in the future, while PFE can manifest the *worst* exposure given a certain confidence level. These two quantities illustrate the loss from both a pricing and risk management perspective [16], respectively. In order to get these metrics of future losses, in practice, the exposure profile needs to be computed for a large number of scenarios on a set of time steps. This is one of the involved parts in computing CVA.

A general Monte Carlo (MC) framework is formulated by Pykhtin and Zhu [30] for the computation of exposure profiles for over-the-counter (OTC) derivative products. There are three basic components: (1) Monte Carlo path generation for a series of simulation dates under some underlying dynamics; (2) valuation of mark-to-market (MtM) values of the contract for each realization at each simulation date, by some numerical method; (3) calculation of exposure for each simulation at each simulation date.

Calculation of exposure profiles asks for efficient numerical methods, as the computational demand grows rapidly w.r.t. the number of MC paths. Different numerical methods have been combined with the MC forward paths to handle the computational demand of exposure, such as the Finite Difference Monte Carlo Method [12] or the Monte Carlo COS method[1] [31]. Computational complexity increases for CVA of a whole portfolio, as there are then multiple financial derivatives in the exposed portfolio. Inclusion of various market factors in the asset dynamics, such as stochastic asset volatility and stochastic interest rates, further increases the computational effort.

We will use the Stochastic Grid Bundling Method (SGBM) for the efficient and flexible computation of exposure. The SGBM technique was proposed for pricing multiple-asset Bermudan derivative contracts under Black-Scholes dynamics in [20]. In the present work we extend SGBM to computing exposure values of options under a stochastic volatility asset equity model with stochastic interest rates. We show the impact of adding stochastic volatility and stochastic interest rates on the metrics of future losses (i.e. CVA, EE, PFE). A stochastic volatility may explain the implied volatility surface observed in the derivatives market (such as the volatility smile) [18], and uncertainty in the interest rate may give a significant contribution to the price, especially of long-term financial derivatives [25]. The

[1]The COS method is an option pricing method for European/Bermudan options based on the Fourier-cosine series developed first by F.Fang and C.W. Oosterlee.

hybrid model chosen to model these stochastic quantities is the Heston Hull-White model [17]. We will also study the impact of stochastic interest rate and stochastic volatility, respectively, under the Black-Scholes Hull-White model and the Heston model.

SGBM is based on *simulation*, *regression*, and *bundling* [20], and the method is very suitable for the computation of exposure profiles. The idea of using simulation and regression for pricing options with early exercise has been used by Carriere [9], Tsitsiklis and Van Roy [33], and Longstaff and Schwartz [27]. There are several recent modifications and comparisons of pricing techniques with regression, such as the work by Broadie and Cao [7], by Broadie et al. [8] and by Stentoft [32]. SGBM distinguishes itself from other regression-based simulation methods in the following ways. First of all, a bundling technique is employed to ensure an accurate *local* calculation of the exposures on each path. Secondly, the conditional expectations of basis functions used for regression in SGBM are analytic expressions when the underlying framework is affine or can be approximated by an affine model. They are used for the calculation of the continuation values. Thirdly, compared to the popular Longstaff-Schwartz (LS) method that uses the 'in-the-money' paths, SGBM uses the information of all paths and assigns exposure values to each path at each monitoring date. These features ensure the accuracy of computing exposure values on each path, which is in particular important for PFE. Furthermore, sensitivities of the EE can be calculated accurately with little extra effort.

The flexibility of SGBM is demonstrated by placing the computation of exposure profiles, for different option types under different asset dynamics, in a general unifying framework based on backward recursion. The options considered include European, Bermudan and barrier options. The reminder of the paper is structured as follows: Sect. 2 provides the mathematical framework for CVA and exposure, discusses the affine diffusion models for the underlying, and the backward dynamics for calculation of the exposure of options, and their exposure sensitivities. In Sect. 3, we present the SGBM algorithm in detail. In Sect. 4 the choice of basis functions and the derivation of the discounted moments is presented, as well as a simple bundling technique that ensures the accuracy of the local, bundle-wise, regression. In Sect. 5, numerical results are presented to show the convergence and efficiency of the method, and the impact of the stochastic interest rate and stochastic volatility on the exposure metrics is studied in Sect. 5.4.

2 CVA and Exposure

CVA is the price of counterparty-credit risk. It is based on an expected value (the expected exposure) which is computed under the risk-neutral measure. There has been debate on the computation of PFE regarding whether to compute it under the real-world or the risk-neutral measure. It is argued that PFE should be computed based on simulations under the real-world measure, reflecting the future developments in the market realistically, from a risk management perspective [22].

In this paper we will focus on the computation of CVA, and we will compute EE and PFE under the risk-neutral measure as well. However, the numerical techniques in this paper can be also be used for computing PFE under the real-world measure, which is a next stage of our work.

The default probability will also be measured under the risk-neutral measure in this paper. The implied default probability of the counterparty typically is retrieved from market prices of CDS (credit default swap) or corporate bonds issued by this counterparty. Notice that the implied default probability under the risk-neutral measure in general is different from that inferred from historical data under the real-world measure, and of the two the former is typically higher than the latter [5].

2.1 Mathematical Formulation

Assuming a market without friction. Let $(\Omega, \mathscr{F}, \mathbb{P})$ be a complete probability space on a finite time horizon $[0, T]$ including all required quantities, where Ω is the sample space, $\mathscr{F}$ is the sigma algebra of events at time T, and $\mathbb{P}$ is the probability measure. We assume the existence of a risk-neutral probability measure $\mathbb{Q}$, equivalent to $\mathbb{P}$, under which the current value of a financial asset is equal to its expected discounted payoff in the future. The uncertainty of the market includes a set of influencing factors, such as the (log-)stock price and its volatility, and the short rate. These quantities can all be expressed by an n-dimensional Markov process $(\mathbf{Y}_t)_{t\in[0,T]}$, $\mathbf{Y}_t = [Y_t^1, Y_t^2, \ldots, Y_t^n]$ in some space $U \subset \mathbb{R}^n$. The natural filtration $(\mathscr{F}_t)_{t\in[0,T]}$ on the probability space is the sigma algebra associated to $\mathbf{Y}_t$, and $\mathscr{F}_t$ includes all information about the market up to time t. We further suppose the existence of a risk-free asset, $B(t) = \exp\left(\int_0^t r_u du\right)$, where $r_t = r(\mathbf{Y}_t)$ is the short rate at time t. The associated stochastic discounting factor in the period $[t, s]$ is defined as $D(t, s) := \exp\left(-\int_t^s r_u du\right)$. The value of a default-free zero coupon bond (ZCB) at time t with maturity T is given by $p(t, T) := \mathbb{E}^{\mathbb{Q}}\left[D(t, T)\middle|\mathscr{F}_t\right]$.

We will study the exposure for investors towards option writers. Particularly, we will compute exposure profiles of OTC Bermudan, European and barrier options, for which the contract values of the options at time t are only determined by the variable $\mathbf{Y}_t$, i.e. the option values can be regarded as functions $V(t, \mathbf{Y}_t) : [0, T] \times U \to \mathbb{R}$. The exposure can also be measured in terms of the *replacement costs* for a derivative contract, i.e. the amount to replace the contract at current market rates [16]. Without transaction costs, the exposure of options in a default event is the loss defined by the replacement costs without any recovery. We assume that the exposure to the writer immediately becomes zero when the option is terminated, exercised or knocked out. Hence, exposure can be expressed by:

$$E(t, \mathbf{Y}_t) = \begin{cases} 0, & \text{if the option is terminated, knocked out or exercised,} \\ V(t, \mathbf{Y}_t), & \text{if the option is alive.} \end{cases} \tag{1}$$

In addition, the *discounted exposure* is defined by $E^*(t, \mathbf{Y}_t) := D(0, t) \cdot E(t, \mathbf{Y}_t)$.

The likelihood of default of the counterparty is another important quantity in the calculation of the CVA. We will utilize the intensity (the so-called reduced form) model, of which the construction has been widely studied. Some work on initial intensity models was presented by Jarrow and Turnbull [21], Madan and Unal [28], Duffie and Singleton [13]. Lando [23] presented the term structure of defaultable bonds with the assumption of independence between the risk-free interest rate and the default intensity. A detailed discussion of intensity modeling of default risk can be found in the books by Bielecki and Rutkowski [3], Lando [23] and Brigo and Mercurio [6].

We also discuss the intensity model briefly here. Let $h_t := h(\mathbf{Y}_t)$ be the $\mathscr{F}_t$-intensity of a jump process and $\tau_d > 0$ be the first jump time of this process. We construct a right continuous process $H_t = \mathbb{1}(\tau_d \leq t)$, where $\mathbb{1}(\cdot)$ is the indicator function. The natural filtration generated by $\mathscr{H}_t$ is given by $\mathscr{H}_t := \sigma(H_s)_{s\in[0,t]}$. The enlarged filtration $\mathscr{G}_t = \mathscr{H}_t \vee \mathscr{F}_t$ thus includes all information of default events and market quantities up to time t. The *survival probability* under the risk-free measure $\mathbb{Q}$ at time t can be expressed by an intensity function:

$$PS(t) = \mathbb{Q}\left(\tau_d > t \middle| \mathscr{G}_t\right) = \mathbb{E}^{\mathbb{Q}}\left[\mathbb{1}\left(\tau_d > t\right) \middle| \mathscr{G}_t\right] = \exp\left(-\int_0^t h_s ds\right), \tag{2}$$

where intensity h_t defines the default probability on a small interval dt when $\tau_d > t$.

By definition, CVA materializes the expected loss in the future, which can be expressed by:

$$\begin{aligned}\text{CVA} &:= \mathbb{E}^{\mathbb{Q}}\left[\text{LGD}\cdot E^*(\tau_d, \mathbf{Y}_{\tau_d}) \middle| \mathscr{G}_0\right] = \int_0^T \mathbb{E}^{\mathbb{Q}}\left[\text{LGD}\cdot E^*(t, \mathbf{Y}_t)\cdot d\left(-PS(t)\right) \middle| \mathscr{G}_0\right] \\ &= \int_0^T \mathbb{E}\left[\text{LGD}\cdot E^*(t, \mathbf{Y}_t)\cdot h_t \cdot \exp\left(-\int_0^t h_s ds\right) \middle| \mathscr{F}_0\right] dt, \end{aligned} \tag{3}$$

where LGD is the loss given default (as a percentage), and the details of derivation of the third equality can be found in [23, p.117].

There are three key elements in the calculation of CVA: the loss given default, the discounted exposure and the survival/default probability of the counterparty. In a real-life situation these three elements are typically not independent. Wrong-way risk (WWR) incurs when the exposure is adversely correlated with the credit quality of the counterparty, which may significantly increase CVA [16]. When assuming independence, the calculation formula of CVA is given by:

$$\text{CVA} = \text{LGD}\int_0^T \mathbb{E}^{\mathbb{Q}}\left[E^*(t, \mathbf{Y}_t) \middle| \mathscr{F}_0\right] d\left(-PS(t)\right), \tag{4}$$

where LGD is assumed to be a fixed ratio based on market information, and the marginal survival probability $PS(t)$ can be obtained via the implied survival probability curve on the CDS market [6].

The well-known quantities of the exposure distribution, EE and PFE, are important for risk management [16]. The mathematical formulas for the EE and PFE quantities are given by:

$$\mathrm{EE}(t) := \mathbb{E}^{\mathbb{Q}}\left[\mathrm{E}(t, \mathbf{Y}_t)\middle|\mathscr{F}_0\right], \tag{5}$$

$$\mathrm{PFE}^{\alpha}(t) := \inf\left\{x\middle|\mathbb{Q}\left\{\mathrm{E}(t, \mathbf{Y}_t) < x\middle|\mathscr{F}_0\right\} > \alpha\right\}, \tag{6}$$

where α is the confidence level. For calculating PFE, the confidence level $\alpha = 97.5\%$ is commonly used to measure the 'worst' losses [16]. Both quantities are deterministic functions in the period $[0, T]$.

2.2 Affine Diffusion Models

For the asset price processes under study here, we will benefit from the affine diffusion (AD) class of Markov stochastic processes $(\mathbf{Y}_t)_{t\in[0,T]}$, which can be expressed by the general form,

$$d\mathbf{Y}_t = \mu\left(\mathbf{Y}_t\right)dt + \sigma(\mathbf{Y}_t)d\widetilde{\mathbf{W}}_t, \tag{7}$$

where $\widetilde{\mathbf{W}}_t$ is an $\mathscr{F}_t$-measurable column vector of independent Wiener processes under measure $\mathbb{Q}$ in $\mathbb{R}^n$, the drift term $\mu\left(\mathbf{Y}_t\right) : U \to \mathbb{R}^n$, and the volatility term $\sigma(\mathbf{Y}_t) : U \to \mathbb{R}^{n\times n}$. In the AD class it is assumed that the drift term, the covariance $\left(\sigma(\mathbf{Y}_t)\sigma(\mathbf{Y}_t)^T\right)$ and the interest rate are of the affine form, i.e.

$$\begin{aligned}
\mu(\mathbf{Y}_t) &= a_0 + a_1\mathbf{Y}_t, \text{ for any } (a_0, a_1) \in \mathbb{R}^n \times \mathbb{R}^{n\times n},\\
\left(\sigma(\mathbf{Y}_t)\sigma(\mathbf{Y}_t)^T\right)_{ij} &= (c_0)_{ij} + (c_1)_{ij}^T\mathbf{Y}_t, \text{ with } (c_0, c_1) \in \mathbb{R}^{n\times n} \times \mathbb{R}^{n\times n\times n},\\
r(\mathbf{Y}_t) &= r_0 + r_1^T\mathbf{Y}_t, \text{ for } (r_0, r_1) \in \mathbb{R} \times \mathbb{R}^n.
\end{aligned} \tag{8}$$

With this type of model, it can be shown that the discounted characteristic function (dChF) is of the following form:

$$\begin{aligned}
\Phi(\mathbf{u}, \mathbf{Y}_t, t, T) &= \mathbb{E}\left[\exp\left(-\int_t^T r_u du + i\mathbf{u}^T\mathbf{Y}_T\right)\middle|\mathscr{F}_t\right]\\
&= \exp\left(A(\mathbf{u}, \tau) + \mathbf{B}^T(\mathbf{u}, \tau)\mathbf{Y}_t\right),
\end{aligned} \tag{9}$$

with time lag $\tau = T - t$. The coefficients satisfy the ODE system [13, 17]

$$\begin{aligned}\frac{d}{d\tau}A(\mathbf{u},\tau) &= -r_0 + \mathbf{B}^T(\mathbf{u},\tau)a_0 + \frac{1}{2}\mathbf{B}^T(\mathbf{u},\tau)c_0\mathbf{B}(\mathbf{u},\tau), \quad A(\mathbf{u},0) = 0,\\ \frac{d}{d\tau}\mathbf{B}(\mathbf{u},\tau) &= -r_1 + a_1^T\mathbf{B}(\mathbf{u},\tau) + \frac{1}{2}\mathbf{B}^T(\mathbf{u},\tau)c_1\mathbf{B}(\mathbf{u},\tau), \quad \mathbf{B}(\mathbf{u},0) = i\mathbf{u}.\end{aligned} \tag{10}$$

The dChF facilitates the calculation of the discounted moments in Sect. 4.1, which is one of the key components within the SGBM algorithm.

Based on this general expression for affine models, we will discuss several hybrid models.

2.2.1 Black-Scholes Hull-White Model and Heston Model

The famous Black-Scholes option pricing partial differential equation (PDE) [4] is based on the assumptions that the asset price follows a geometric Brownian motion with constant volatility and constant interest rate. We first relax the assumption of constant interest rate by a stochastic instantaneous short-rate r_t. In practice, interest rates vary over time and by tenor T, as observed in the zero coupon bond curves in the market [6]. The instantaneous forward rate at time t for a maturity $T > t$ is defined by:

$$f(t,T) := -\frac{\partial \log p(t,T)}{\partial T}. \tag{11}$$

The characterization of the term structure of interest rates is well-known from Vasicek [34], Cox, Ingersoll, and Ross [11], and Hull and White [19]. In this paper, we will also employ the *Black-Scholes Hull-White* hybrid (BSHW) model. Under risk-neutral measure $\mathbb{Q}$, the dynamics of the model $\mathbf{Y}_t = [x_t, r_t]^T$ are given by the following SDEs [6]:

$$\begin{aligned}dx_t &= \left(r - \frac{1}{2}\sigma^2\right)dt + \sigma dW_t^x,\\ dr_t &= \lambda(\theta(t) - r_t)dt + \eta dW_t^r,\end{aligned} \tag{12}$$

where $x_t = \log(S_t)$ represents the log-asset variable; the two correlated Wiener processes (W_t^x, W_t^r) are defined by $W_t^x = \widetilde{W}_t^{(1)}$ and $W_t^r = \rho_{x,r}\widetilde{W}_t^{(1)} + \sqrt{1-\rho_{x,r}^2}\widetilde{W}_t^{(2)}$, where $\widetilde{W}_t^{(1)}$ and $\widetilde{W}_t^{(2)}$ are two independent standard Wiener processes under measure $\mathbb{Q}$ and $|\rho_{x,r}| < 1$ is the instantaneous correlation parameter between the asset price and the short rate process; positive parameters σ and η denote the volatility of equity and interest rate, respectively; the drift term $\theta(t)$ is a deterministic function chosen to fit the term structure observed in the market, which must satisfy:

$$\theta(t) = f(0,t) + \frac{1}{\lambda}\frac{\partial}{\partial t}f(0,t) + \frac{\eta^2}{2\lambda^2}(1 - \exp(-2\lambda t)). \tag{13}$$

Another way of extending the Black-Scholes model is to define the variance as a diffusion process, like in the stochastic volatility model developed by Heston [18]. With state variable $\mathbf{Y}_t = [x_t, v_t]^T$, the Heston model is given by:

$$\begin{aligned} dx_t &= \left(r - \frac{1}{2}v_t\right)dt + \sqrt{v_t}dW_t^x, \\ dv_t &= \kappa(\bar{v} - v_t)dt + \gamma\sqrt{v_t}dW_t^v, \end{aligned} \tag{14}$$

where r is a constant interest rate; the two correlated Wiener processes (W_t^x, W_t^v) are defined by $W_t^x = \widetilde{W}_t^{(1)}$ and $W_t^v = \rho_{x,v}\widetilde{W}_t^{(1)} + \sqrt{1-\rho_{x,v}^2}\widetilde{W}_t^{(3)}$, where $\widetilde{W}_t^{(1)}$ and $\widetilde{W}_t^{(3)}$ are two independent standard Wiener processes under measure $\mathbb{Q}$ and $|\rho_{x,v}| < 1$ is the instantaneous correlation parameter between the asset price and the variance process; the constant positive parameters κ, $\bar{v}$, γ determine the reverting speed, the reverting level and vol-of-vol parameters, respectively. The associated PDE can be found in [18, p. 329].

2.2.2 Heston Hull-White Model and H1HW Model

Consider a state vector including all these stochastic quantities, i.e. $\mathbf{Y}_t = [x_t, v_t, r_t]^T$. The corresponding model can be defined by adding a HW interest rate process to the Heston stochastic volatility dynamics, as presented in [17]. The hybrid model of the equity, stochastic Heston asset volatility and stochastic interest rate is represented by the following SDEs:

$$\begin{aligned} dx_t &= \left(r_t - \frac{1}{2}v_t\right)dt + \sqrt{v_t}dW_t^x, \\ dv_t &= \kappa(\bar{v} - v_t)dt + \gamma\sqrt{v_t}dW_t^v, \\ dr_t &= \lambda(\theta(t) - r_t)dt + \eta dW_t^r, \end{aligned} \tag{15}$$

where the correlated Wiener processes (W_t^x, W_t^v, W_t^r) are defined by $W_t^x = \widetilde{W}_t^{(1)}$, $W_t^v = \rho_{x,v}\widetilde{W}_t^{(1)} + \sqrt{1-\rho_{x,v}^2}\widetilde{W}_t^{(2)}$, $W_t^r = \rho_{x,r}\widetilde{W}_t^{(1)} - \frac{\rho_{x,v}\rho_{x,r}}{\sqrt{1-\rho_{x,v}^2}}\widetilde{W}_t^{(2)} + \sqrt{\frac{1-\rho_{x,v}^2-\rho_{x,r}^2}{1-\rho_{x,v}^2}}\widetilde{W}_t^{(3)}$, in which $\widetilde{W}_t^{(1)}$, $\widetilde{W}_t^{(2)}$ and $\widetilde{W}_t^{(3)}$ are three independent standard Wiener processes under the risk-neutral measure $\mathbb{Q}$, and $\rho_{x,v}$ and $\rho_{x,r}$ are correlation parameters that satisfy $\rho_{x,v}^2 + \rho_{x,r}^2 < 1$; the parameters λ, $\theta(t)$, η are as in (12), and κ, $\bar{v}$ and γ are as in (14); the initial values satisfy $r_0 > 0$ and $v_0 > 0$.

The Heston Hull-White (HHW) SDE system in (15) is not affine. Conditioned on information at time t, the symmetric covariance matrix at time $s > t$ is given by:

$$\sigma\left(\mathbf{Y}_s\right)\sigma\left(\mathbf{Y}_s\right)^T = \begin{pmatrix} v_s & \rho_{x,v}v_s & \sqrt{v_s}\eta\rho_{x,r} \\ * & \gamma^2 v_s & 0 \\ * & * & \eta^2 \end{pmatrix}. \tag{16}$$

where the term $\sqrt{v_s}$ is not linear. Grzelak and Oosterlee in [17] approximated the covariance matrix in (16) by

$$\sigma\left(\mathbf{Y}_s\right)\sigma\left(\mathbf{Y}_s\right)^T \approx \hat{\sigma}\left(\mathbf{Y}_s\right)\hat{\sigma}\left(\mathbf{Y}_s\right)^T = \begin{pmatrix} v_s & \rho_{x,v}v_s & \mathbb{E}\left[\sqrt{v_s}\middle|v_t\right]\eta\rho_{x,r} \\ * & \gamma^2 v_s & 0 \\ * & * & \eta^2 \end{pmatrix}, \tag{17}$$

where the term $\sqrt{v_s}$ is approximated by its conditional expectation $\mathbb{E}\left[\sqrt{v_s}\middle|v_t\right]$, for which an analytic formula is given by:

$$\mathbb{E}\left[\sqrt{v_s}\middle|v_t\right] = \sqrt{2c(\tau_1)}e^{-\frac{\bar{\lambda}(\tau_1,v_t)}{2}}\sum_{k=0}^{\infty}\frac{1}{k!}\left(\frac{\bar{\lambda}(\tau_1,v_t)}{2}\right)^k\frac{\Gamma\left(\frac{1+d}{2}+k\right)}{\Gamma\left(\frac{d}{2}+k\right)}, \tag{18}$$

with $\tau_1 := s - t$, and

$$c(\tau_1) = \frac{1}{4\kappa}\gamma^2(1-e^{-\kappa\tau_1}), \quad d = \frac{4\kappa\bar{v}}{\gamma^2}, \quad \bar{\lambda}(\tau_1,v_t) = \frac{4\kappa v_t e^{-\kappa\tau_1}}{\gamma^2(1-e^{-\kappa\tau_1})}. \tag{19}$$

This affine approximation of the HHW model with covariance (17) is called the H1HW model, and details can be found in [17]. In this paper, we further make an approximation of the calculation in (18), as presented in Appendix 3.

2.3 *Pricing European, Bermudan and Barrier Options*

We will study the CVA, EE and PFE of several types of options to show the flexibility of SGBM. We present the backward valuation dynamics framework for European, Bermudan and barrier options in this section. Let the collection of equally-spaced discrete monitoring dates be:

$$\mathscr{T} = \{0 = t_0 < t_1 < \cdots < t_M = T, \Delta t = t_{m+1} - t_m\}.$$

The options will be valued at so-called monitoring dates to determine the exposure profiles. The received payoff from immediate exercise of the option at time t_m is given by

$$g(S_m) := \max\left(\omega(S_m - K), 0\right), \quad \text{with} \begin{cases} \omega = 1, & \text{for a call;} \\ \omega = -1, & \text{for a put,} \end{cases} \tag{20}$$

where K is the strike value and S_m is the underlying asset variable at time t_m.

The *continuation value* of the option at time t_m can be expressed by the conditional expectation of the discounted option value at time t_{m+1}. As we have assumed the Markov property of the process $\mathbf{Y}_m$, we replace the filtration $\mathscr{F}_m$ in the conditional expectation, i.e. the continuation values of the option will be written as a function of the state variable $\mathbf{Y}_m$, i.e.

$$c(t_m, \mathbf{Y}_m) := \mathbb{E}^{\mathbb{Q}}\left[D\left(t_m, t_{m+1}\right) \cdot V(t_{m+1}, \mathbf{Y}_{m+1}) \middle| \mathbf{Y}_m \right], \tag{21}$$

where $\mathbf{Y}_m$ is the state variable at time t_m, and $V(t_{m+1}, \mathbf{Y}_{m+1})$ is the option value at time t_{m+1}.

2.3.1 Bermudan Options

Bermudan options can be exercised at a series of time points before expiry date T. Denote the set of early-exercise dates by $\mathscr{T}_{\mathrm{E}}$. We will take a small step size Δt when simulating the market variables to enhance the accuracy of the CVA calculation, and we assume that the Bermudan option can only be exercised at some of these dates, i.e. $\mathscr{T}_{\mathrm{E}} \subset \mathscr{T}$.

We also assume that the option holder makes the exercise strategy aiming for the 'optimal' profit, and the option holder is not influenced by the credit quality of the option writer when making the decision. We further denote the optimal stopping time by τ_B, which is the optimal time to exercise the option under the assumptions. It should maximize the expected payoff at time $t = 0$, i.e.

$$V^{\mathrm{Berm}}(t_0, \mathbf{Y}_0) = \max_{\tau_B \in \mathscr{T}_{\mathrm{E}}} \mathbb{E}\left[D(0, \tau_B) \cdot g(S_{\tau_B}) \middle| \mathbf{Y}_0 \right]. \tag{22}$$

The essential idea of pricing Bermudan options by simulation is to determine the optimal exercise strategy for each path. At each exercise date, the option holder compares the received payoff from immediate exercise with the expected payoff from continuation of the option to determine the optimal exercise strategy. The dynamics of pricing Bermudan options in backward induction derived by the Snell envelope [14, 27] can be expressed by:

$$V^{\mathrm{Berm}}(t_m, \mathbf{Y}_m) = \begin{cases} g(S_M) & \text{for } t_M = T, \\ \max\left\{c(t_m, \mathbf{Y}_m), g(S_m)\right\}, & \text{for } t_m \in \mathscr{T}_{\mathrm{E}}, \\ c(t_m, \mathbf{Y}_m), & \text{for } t_m \in \mathscr{T} - \mathscr{T}_{\mathrm{E}}. \end{cases} \tag{23}$$

2.3.2 European Options

Similar to pricing Bermudan options, the exposure profile of a European option can be determined based on simulation. The European option value at time T equals the received payoff $V^{\text{Euro}}(t_M, \mathbf{Y}_M) = g(S_M)$; at time points $t_m < T$, the value of the European option is equal to the discounted conditional expected payoff, i.e.,

$$V^{\text{Euro}}(t_m, \mathbf{Y}_m) := \mathbb{E}\left[D(t_m, t_M) \cdot g(S_M) \middle| \mathbf{Y}_m\right], \tag{24}$$

where $g(S_M)$ is the received payoff at time $t_M = T$. By the tower property of expectations, it can be calculated in a backward iteration as:

$$\begin{aligned} V^{\text{Euro}}(t_m, \mathbf{Y}_m) &= \mathbb{E}\left[D(t_m, t_{m+1}) \cdot \mathbb{E}\left[D(t_{m+1}, t_M) \cdot g(S_M) \middle| \mathbf{Y}_{m+1}\right] \middle| \mathbf{Y}_m \right] \\ &= \mathbb{E}\left[D(t_m, t_{m+1}) \cdot V^{\text{Euro}}(t_{m+1}, \mathbf{Y}_{m+1}) \middle| \mathbf{Y}_m \right] = c(t_m, \mathbf{Y}_m). \end{aligned} \tag{25}$$

2.3.3 Barrier Options

Barrier options become active/knocked out when the underlying asset reaches a predetermined level, i.e. the *barrier* level. There are four main types of barrier options: up-and-out, down-and-out, up-and-in, down-and-in options. Here we focus on the *down-and-out* barrier options. A down-and-out barrier option is active initially and gets knocked out (looses its value except for some rebate value) when the underlying hits the barrier; otherwise if the option is not knocked out during its lifetime, the holder will receive the payoff value at the expiry date T. The backward pricing dynamics of the down-and-out barrier options are thus given by [14],

$$V^{\text{barr}}(t_m, \mathbf{Y}_m) = \begin{cases} g(S_m) \cdot \mathbb{1}_{\{S_m > L\}} + r_b \cdot \mathbb{1}_{\{S_m \le L\}}, & \text{for } t_M = T, \\ c(t_m, \mathbf{Y}_m) \cdot \mathbb{1}_{\{S_m > L\}} + r_b \cdot \mathbb{1}_{\{S_m \le L\}}, & \text{for } t_m < T, \end{cases} \tag{26}$$

where $\mathbb{1}(\cdot)$ is the indicator function, L is the barrier level and r_b is the rebate value.

3 The Stochastic Grid Bundling Method (SGBM)

Monte Carlo simulation plays a primary role in computing CVA, i.e. generating N independent scenarios for each monitoring date $\mathscr{T}$. We denote the realization of the state vector $\mathbf{Y}_m$ on the i-th path at time t_m by $\hat{\mathbf{y}}_m(i)$, $i = 1, \ldots, N$. After finishing the calculation of the exposure profile on the generated stochastic grid, the CVA, assuming independence of exposures and defaults, can be computed by the following discrete formula:

$$\text{CVA} \approx \text{LGD} \sum_{m=0}^{M-1} \frac{1}{N} \sum_{i=1}^{N} \left(\exp\left(-\sum_{k=0}^{m-1} r(\hat{\mathbf{y}}_k(i)) \Delta t \right) \cdot E(t_m, \hat{\mathbf{y}}_m(i)) \right) \cdot \Big(PS(t_m) - PS(t_{m+1}) \Big). \tag{27}$$

Similarly, the value at time t_m of the EE and PFE functions can be approximated by:

$$\text{EE}(t_m) \approx \frac{1}{N} \sum_{i=1}^{N} E(t_m, \hat{\mathbf{y}}_m(i)), \tag{28}$$

$$\text{PFE}(t_m) \approx \text{quantile}(E(t_m, \hat{\mathbf{y}}_m(i)), 97.5\%), \tag{29}$$

where the confidence level is set to $\alpha = 97.5\%$.

At expiry date $t_M = T$, the option values on each path can be computed immediately by the received payoff values. The key problem is to calculate the continuation values on each path in the backward algorithm at each monitoring time $t_m < T$, $m = 0, 1, \ldots, M-1$. SGBM combines regression and bundling techniques to compute these expected values.

3.1 Calculation of the Continuation Values

At time $t_m < T$, the generated paths are clustered into some non-overlapping bundles with as a criterion that the realizations $\hat{\mathbf{y}}_m(i)$ on paths within the same bundle should share similar values. The indices of the paths in the j-th bundle are in a set $\mathscr{B}_m^j$, $j = 1, 2, \ldots, J$, where J is the number of bundles. The realizations $\hat{\mathbf{y}}_m(i)$ of the state vector $\mathbf{Y}_m$ within the j-th bundle form a bounded domain $\mathbf{I}_m^j \subset \mathbb{R}^n$, when $m = 1, 2, \ldots, M-1$, given by

$$\mathbf{I}_m^j = \prod_{l=1}^{n} \left[\max_{i \in \mathscr{B}_m^{j-1}} \left(\hat{y}_m^{(l)}(i) \right), \max_{i \in \mathscr{B}_m^j} \left(\hat{y}_m^{(l)}(i) \right) \right], \tag{30}$$

where $\hat{y}_m^{(l)}(i)$ represents the l-th dimension of the realization $\hat{\mathbf{y}}(i)$, and $j = 2, 3, \ldots, J$. When $j = 1$ we define the realized domain $\mathbf{I}_m^1 = \prod_{l=1}^{n} \left[\min_{i \in \mathscr{B}_m^1} \left(\hat{y}_m^{(l)}(i) \right), \max_{i \in \mathscr{B}_m^1} \left(\hat{y}_m^{(l)}(i) \right) \right]$.

These subdomains $\{\mathbf{I}_m^j\}_{j=1}^J$ are disjoint. At the same time, the corresponding realizations $\hat{\mathbf{y}}_{m+1}(i)$ of the state vector $\mathbf{Y}_{m+1}$ within the j-th bundle also form a bounded domain in $\mathbb{R}^n$, i.e.

$$\mathbf{U}_{m+1}^j = \prod_{l=1}^{n} \left[\min_{i \in \mathscr{B}_m^j} \left(\hat{y}_{m+1}^{(l)}(i) \right), \max_{i \in \mathscr{B}_m^j} \left(\hat{y}_{m+1}^{(l)}(i) \right) \right], \tag{31}$$

where $\hat{y}_{m+1}^{(l)}(i)$ represents the l-th dimension of the realization $\hat{\mathbf{y}}_{m+1}(i)$. These domains typically overlap.

We assume that the option function $V(t_{m+1}, \cdot)$ is an element of the L^2 space on the finite domain $\mathbf{U}_{m+1}^j$, i.e. it is square-integrable over $\mathbf{U}_{m+1}^j$ with some measure. Suppose that we have the values of this option function w.r.t. the realizations $\hat{\mathbf{y}}_{m+1}(i)$ on all paths, denoted by $\hat{v}_{m+1}(i)$, $i = 1, 2, \ldots, N$. Given the set of points $\{(\hat{\mathbf{y}}_{m+1}(i), \hat{v}_{m+1}(i))\}_{i=1}^N$, $i \in \mathscr{B}_m^j$, a commonly used approximation of the option function is a constructed function that is the 'best fit' for the data set in least squares sense. With a set of some basis functions $\{\phi_k\}_{k=1}^H$ in L_2, the option function can be approximated on $\mathbf{U}_{m+1}^j$ by a linear combination of the basis functions:

$$V(t_{m+1}, \mathbf{Y}_{m+1}) \approx Z_1(t_{m+1}, \mathbf{Y}_{m+1}) := \sum_{k=1}^{H} \beta_m^j(k) \phi_k(\mathbf{Y}_{m+1}), \tag{32}$$

where H is the number of basis functions, and $\beta_m^j(k)$ are the constant coefficients at time t_m of the k-th basis function ϕ_k within the j-th bundle $\mathscr{B}_m^j$, determined by regression:

$$\underset{\beta_m^j(k) \in \mathbb{R}, k=1,\ldots,H}{\arg\min} \sum_{i \in \mathscr{B}_m^j} \left(\hat{v}_{m+1}(i) - \sum_{k=1}^{H} \beta_m^j(k) \phi_k(\hat{\mathbf{y}}_{m+1}(i)) \right)^2, \tag{33}$$

of which the solution is denoted by $\{\hat{\beta}_m^j(k)\}_{k=1}^H$. Within the j-th bundle, the approximation of the option function on $\mathbf{U}_{m+1}^j$ is thus given by:

$$V(t_{m+1}, \mathbf{Y}_{m+1}) \approx Z_2(t_{m+1}, \mathbf{Y}_{m+1}) := \sum_{k=1}^{H} \hat{\beta}_m^j(k) \phi_k(\mathbf{Y}_{m+1}). \tag{34}$$

Hence the continuation function on the bounded domain $\mathbf{I}_m^j$ can be approximated by a linear combination of the conditional expected discounted basis functions defined by:

$$\begin{aligned} c_2(t_m, \mathbf{Y}_m) &:= \mathbb{E}^{\mathbb{Q}} \left[D(t_m, t_{m+1}) \cdot Z_2(t_{m+1}, \mathbf{Y}_{m+1}) \middle| \mathbf{Y}_m \right] \\ &= \sum_{k=1}^{H} \hat{\beta}_m^j(k) \psi_k(\mathbf{Y}_m, \Delta t), \end{aligned} \tag{35}$$

where the conditional expectation of the k-th discounted basis function is given by

$$\psi_k(\mathbf{Y}_m, \Delta t) := \mathbb{E}^{\mathbb{Q}} \left[D(t_m, t_{m+1}) \cdot \phi_k(\mathbf{Y}_{m+1}) \middle| \mathbf{Y}_m \right]. \tag{36}$$

We will approximate the 'real' continuation function $c(t_m, \cdot)$ given in equation (21) by the function $c_2(t_m, \cdot)$ defined in equation (35) on the bounded domain $\mathbf{I}_m^j$. When analytic formulas of the functions $\{\psi_k\}_{k=1}^H$ defined in (36) are available, the continuation value w.r.t. realization $\hat{\mathbf{y}}_m(i)$ on the i-th path within the j-th bundle can be easily computed by:

$$c(t_m, \hat{\mathbf{y}}_m(i)) \approx c_2(t_m, \hat{\mathbf{y}}_m(i)) = \sum_{k=1}^{H} \hat{\beta}_m^j(k)\psi_k(\hat{\mathbf{y}}_m(i), \Delta t). \tag{37}$$

In addition, we will show that the error of approximation of the continuation function at time t_m is bounded by the error of approximation of the option function at time t_{m+1} in Sect. 3.4.

3.2 Backward Algorithm

From Sect. 3.1, it is clear that the continuation values on each path at time t_m can be calculated in backward fashion as long as the option values at these paths at time t_{m+1} are available. In this section, we will present the backward algorithm of the SGBM for computing exposures of options, first for Bermudan options.

Initializing: At time $t_M = T$, the option values $\{\hat{v}_M(i)\}_{i=1}^N$ on all paths can be calculated from the received payoff.

Backward iteration: At time $t_m < T$, $m = M-1, M-2, \ldots, 1$,

- Step I: apply a bundling technique to cluster all paths into non-overlapping bundles, indexed by $\mathscr{B}_m^j$, $j = 1, 2, \ldots, J$.
- Step II: within the j-th bundle, $j = 1, 2, \ldots, J$, utilize the regression technique to calculate the continuation values at time t_m by:
  - Step (i): approximate coefficients $\{\hat{\beta}_m^j(k)\}_{k=1}^H$ within the j-th bundle by formula (33);
  - Step (ii): calculate continuation values on each path by formula (35) using the approximated coefficients obtained in Step (i).
- Step III: determine option values $\{\hat{v}_m(i)\}_{i=1}^N$ on all paths at time t_m by formula (23) using the approximated continuation values obtained in Step (ii).
- Step IV: determine exposure values at time t_m by formula (1) on each path: if the option at a path is exercised at time t_m, then the corresponding exposure values from time t_m to time t_M at this path are assigned value zero; otherwise the exposure values are the computed continuation values on the path.

Finalizing: At time $t_0 = 0$, approximate directly the coefficients $\{\hat{\beta}_m(k)\}_{k=1}^H$ and calculate the continuation value at time t_0, which is also the option value at time t_0.

The backward algorithm of calculating the exposure profile of a European option or a barrier option is the same as the algorithm for a Bermudan option, except that the pricing formula (23) in Step III needs to be replaced by formula (25) for pricing European options or formula (26) for pricing barrier options, respectively.

3.3 Sensitivities of EE

The sensitivities *Delta* (Δ_{EE}) and *Gamma* (Γ_{EE}) of EE w.r.t. the change of the underlying asset price S_0 can be computed in the same backward algorithm for the computation of the exposure profile. At time $t_M = T$, we simply assign value zero to these derivatives of the EE function. At time $t_m < T$, the sensitivities can be computed by:

$$\Delta_{\mathrm{EE}}(t_m) := \frac{\partial \mathrm{EE}}{\partial S_0}(t_m) \approx \frac{1}{N}\sum_{i=1}^{N} \frac{\partial \mathrm{E}}{\partial x_m}(t_m, \hat{\mathbf{y}}_m(i)) \cdot \frac{1}{S_0}, \tag{38}$$

$$\Gamma_{\mathrm{EE}}(t_m) := \frac{\partial^2 \mathrm{EE}}{\partial S_0^2}(t_m) \approx \frac{1}{N}\sum_{i=1}^{N} \left(\frac{\partial^2 \mathrm{E}}{\partial x_m^2}(t_m, \hat{\mathbf{y}}_m(i)) - \frac{\partial \mathrm{E}}{\partial x_m}(t_m, \hat{\mathbf{y}}_m(i)) \right) \cdot \frac{1}{S_0^2}, \tag{39}$$

where $x_m = \log(S_m)$ represents the log-asset value at time t_m. The derivation of formulas (38) and (39) is presented here. At time t_m, the first derivative of the EE function can be computed by

$$\frac{\partial \mathrm{EE}}{\partial S_0}(t_m) \approx \frac{1}{N}\sum_{i=1}^{N} \frac{\partial \mathrm{E}}{\partial S_0}(t_m, \hat{\mathbf{y}}_m(i)), \tag{40}$$

by the chain rule,

$$\frac{\partial \mathrm{E}}{\partial S_0}(t_m, \hat{\mathbf{y}}_m(i)) = \frac{\partial \mathrm{E}}{\partial x_m} \cdot \frac{\partial x_m}{\partial S_m} \cdot \frac{\partial S_m}{\partial S_0}(t_m, \hat{\mathbf{y}}_m(i)), \tag{41}$$

where $x_m := \log S_m$, and

$$\frac{\partial x_m}{\partial S_m} = \frac{1}{S_m}, \quad \frac{\partial S_m}{\partial S_0} = \frac{S_m}{S_0}. \tag{42}$$

The second equation in (42) can be derived as follows. The asset value S_t follows a Geometric Brownian motion process, i.e.

$$d \log S_t = \mu_t dt + \sigma_t dW_t. \tag{43}$$

By integrating both sides, we obtain

$$S_t = S_0 \cdot \exp\left(\int_0^t (\mu_s ds + \sigma_s dW_s)\right), \tag{44}$$

hence the derivative of S_t w.r.t. S_0 can be expressed by

$$\frac{\partial S_t}{\partial S_0} = \exp\left(\int_0^t (\mu_s ds + \sigma_s dW_s)\right) = \frac{S_t}{S_0}. \tag{45}$$

So, the first derivative of the EE function can be expressed by

$$\frac{\partial \mathrm{EE}}{\partial S_0}(t_m) \approx \frac{1}{N}\sum_{i=1}^{N} \frac{\partial \mathrm{E}}{\partial x_m}(t_m, \hat{\mathbf{y}}_m(i)) \cdot \frac{1}{S_0}. \tag{46}$$

From (46), the second derivative can be derived by

$$\begin{aligned}\frac{\partial^2 \mathrm{EE}}{\partial S_0^2}(t_m) &= \frac{1}{N}\sum_{i=1}^{N}\left(\frac{\partial \mathrm{E}}{\partial x_m^2}(t_m, \hat{\mathbf{y}}_m(i)) \cdot \frac{x_m}{S_m}\cdot\frac{S_m}{S_0}\cdot\frac{1}{S_0} + \frac{\partial \mathrm{E}}{\partial x_m}(t_m, \hat{\mathbf{y}}_m(i)) \cdot \left(-\frac{1}{S_0^2}\right)\right)\\ &= \frac{1}{N}\sum_{i=1}^{N}\left(\frac{\partial^2 \mathrm{E}}{\partial x_m^2}(t_m, \hat{\mathbf{y}}_m(i)) - \frac{\partial \mathrm{E}}{\partial x_m}(t_m, \hat{\mathbf{y}}_m(i))\right)\cdot\frac{1}{S_0^2}.\end{aligned} \tag{47}$$

For those paths on which the option is alive at time t_m, the first and the second derivatives of the exposure function are given by

$$\begin{aligned}\frac{\partial \mathrm{E}}{\partial x_m}(t_m, \mathbf{Y}_m) &:= \frac{\partial c}{\partial x_m}(t_m, \mathbf{Y}_m),\\ \frac{\partial^2 \mathrm{E}}{\partial x_m^2}(t_m, \mathbf{Y}_m) &:= \frac{\partial^2 c}{\partial x_m^2}(t_m, \mathbf{Y}_m),\end{aligned} \tag{48}$$

where the derivatives of the continuation function w.r.t. x_m within the j-th bundle are approximated by

$$\begin{aligned}\frac{\partial c}{\partial x_m}(t_m, \mathbf{Y}_m) &\approx \sum_{k=1}^{H} \hat{\beta}_m^j(k)\frac{\partial \psi_k}{\partial x_m}(\mathbf{Y}_m, \Delta t),\\ \frac{\partial^2 c}{\partial x_m^2}(t_m, \mathbf{Y}_m) &\approx \sum_{k=1}^{H} \hat{\beta}_m^j(k)\frac{\partial^2 \psi_k}{\partial x_m^2}(\mathbf{Y}_m, \Delta t),\end{aligned} \tag{49}$$

with the same coefficient set $\{\hat{\beta}_m^j(k)\}_{k=1}^H$ as in (35).

For those paths on which the option has been exercised or knocked out at time t_m, the derivatives of EE are given value zero, as the exposure values on these paths are zero.

3.4 Convergence Results

The so-called *direct estimator* is obtained in the backward algorithm by regression [20]. With convexity of the 'max' function, it can be proven by induction that the direct estimator is often higher than the true value with some bias, and that the direct estimator converges to the option value as the number of paths and the number of monomial basis functions goes to infinity. See Theorem 2 and Theorem 4 in [20].

In addition, an estimator can be made based on the average cash flow of a second set of paths, referred to as the *path estimator*. Using the coefficients obtained by regression based on one set of paths, an approximation of the optimal early exercise strategy of another set of paths can be made by comparing values of continuation and values of immediate exercise. The path estimator is often a lower bound of the option value, converging a.s. as the number of paths goes to infinity [20], since the option value computed by the optimal early exercise strategy is the supremum of the option value at time $t = 0$ by definition. Details of the proof can be found in [20, 27].

For European and barrier options, one can take the discounted average of the MC paths as our reference. For Bermudan options, the direct and path estimators provide a conservative confidence interval for the true option value [20]:

$$\left[V^{\text{path}}(0) - 1.96\frac{\hat{s}_{\text{path}}}{\sqrt{N_s}}, V^{\text{direct}}(0) + 1.96\frac{\hat{s}_{\text{direct}}}{\sqrt{N_s}} \right], \tag{50}$$

where $\hat{s}_{\text{path}}$ and $\hat{s}_{\text{direct}}$ are the sample standard deviations for the path and direct estimator respectively, and $V^{\text{path}}(0)$ and $V^{\text{direct}}(0)$ are the sample means of the path and direct estimators respectively; these sample means and sample standard deviations are based on N_s independent trials.

The approximation of the option function converges as the number of paths, the number of basis functions and the number of bundles go to infinity. Details of this can be found in Appendix 4. From the discussion of convergence in Appendix 4, we can also conclude that by using bundles, the option function can be approximated well piece-wise functions, even with a low order $p = 1$. This advantage of the SGBM approach will reduce the computational effort for increasing problem dimensions. In addition, the error of approximation of the continuation function can be uniformly bounded by the error in approximating the option function, as stated in Proposition 1. It ensures the accuracy of the computed continuation values by SGBM on each path, which is important for computing exposure profiles.

Proposition 1 *At time t_m, the error of approximating the continuation function by SGBM is uniformly bounded by the error of approximation of the option function within each bundle, given by*

$$\begin{aligned}\left|c(t_m,\mathbf{Y}_m)-c_2(t_m,\mathbf{Y}_m)\right| &\leq \|V(t_{m+1},\cdot)-Z_2(t_{m+1},\cdot)\|_{L_2}\\ &= \left(\int_{\mathbf{Y}_{m+1}\in\mathbb{R}^n}\left(V(t_{m+1},\mathbf{Y}_{m+1})-Z_2(t_{m+1},\mathbf{Y}_{m+1})\right)^2 d\mu_{(\mathbf{Y}_{m+1}|\mathbf{Y}_m)}\right)^{\frac{1}{2}}, \quad (51)\end{aligned}$$

where $\mu_{(\mathbf{Y}_{m+1}|\mathbf{Y}_m)}$ is the probability measure conditioned on $\mathbf{Y}_m \in \mathbf{I}_m^j$ under the risk-neutral measure $\mathbb{Q}$.

Proof By Jensen's inequality it is proved in Appendix 5.

4 Choice of Basis Functions and Bundling

4.1 The Monomial Basis and the Discounted Moments

Essentially, the approximation of the option function expressed in (32) is its projection onto a space consisting of basis functions on the bounded domain $\mathbf{U}_{m+1}^j$. For the polynomial space, it is natural to take *monomials* as the basis, as all monomials with order lower or equal to any degree $p \in \mathbb{N}$ can form a closure. With a state vector $\mathbf{Y}_t = [Y_t^1, Y_t^2, \ldots, Y_t^l, \ldots, Y_t^n] \in \mathbb{R}^n$, a monomial basis of order $p > 0$ can be expressed by $\prod_{l=1}^{n}\left(Y_t^l\right)^{q_l}$, where $\left(\sum_{l=1}^{n} q_l\right) = p$, with $q_l \geq 0$ for any l. The number of basis functions of a monomial basis of order less than or equal to p is $H = \frac{(n+p)!}{p!n!}$. We denote the polynomial space of order p on the bounded domain $\mathbf{U}_{m+1}^j$ by:

$$\mathscr{P}(\mathbf{U}_{m+1}^j, p) := \left\{ f \middle| f(\mathbf{y}) = \sum_{k=1}^{H} \beta(k)\phi_k(\mathbf{y}),\ \mathbf{y} \in \mathbf{U}_{m+1}^j,\ \boldsymbol{\beta} \in \mathbb{R}^H. \right\}, \quad (52)$$

where $\boldsymbol{\beta} := [\beta(1), \beta(2), \cdots, \beta(H)] \in \mathbb{R}^H$, and $\{\phi_k\}_{k=1}^H$ is the monomial basis. Table 1 presents the monomial basis set for the hybrid models in this paper with degree $p = \{1, 2, 3\}$.

The monomial basis grows rapidly with the dimension of the state variable n and the polynomial order p. In the algorithm of SGBM, bundling will enhance the accuracy and thus a lower degree p can be employed to achieve a certain accuracy level, as we will see in the numerical Sect. 5.

Table 1 The monomial basis for the hybrid models

order p	Heston	BSHW	HHW $\rightarrow$H1HW
1	$\{1, x_t, v_t\}$	$\{1, x_t, r_t\}$	$\{1, x_t, v_t, r_t\}$
2	$\{1, x_t, v_t, x_t^2, x_t v_t, v_t^2\}$	$\{1, x_t, r_t, x_t^2, x_t r_t, r_t^2\}$	$\{1, x_t, v_t, r_t, x_t^2, x_t v_t, v_t^2, x_t r_t, r_t^2, v_t r_t\}$
3	$\{1, x_t, v_t, x_t^2, x_t v_t, v_t^2, x_t^3, x_t^2 v_t, x_t v_t^2, v_t^3\}$	$\{1, x_t, r_t, x_t^2, x_t r_t, r_t^2, x_t^3, x_t^2 r_t, x_t r_t^2, r_t^3\}$	

The expected value of a discounted monomial basis is the *discounted moment*, for which an analytic formula, the ψ-function, is needed in the calculation of the continuation function. Over a time period $[s, t]$, the k-th discounted moment of an n-dimensional vector $\mathbf{Y}_t$, corresponding to the monomial basis $\prod_{l=1}^{n} \left(Y_t^l\right)^{q_l}$ with degree $0 \leq \left(\sum_{l=1}^{n} q_l\right) \leq p$, is defined by:

$$\psi_k(\mathbf{Y}_s, t-s) := \mathbb{E}^{\mathbb{Q}}\left[\prod_{l=1}^{n} \left(Y_t^l\right)^{q_l} \cdot D(s,t) \middle| \mathbf{Y}_s\right], \tag{53}$$

which can be derived by the associated dChF of the dynamics,

$$\psi_k(\mathbf{Y}_s, t-s) = \frac{1}{(i)^p} \prod_{l=1}^{n} \frac{\partial^{q_l} \Phi}{\partial u_l^{q_l}}(\mathbf{u}; \mathbf{Y}_s, t-s)\Big|_{\mathbf{u}=\mathbf{0}}, \tag{54}$$

where i represents the imaginary unit, vector $\mathbf{u} = [u_1, u_2, \ldots, u_l, \ldots, u_n] \in \mathbb{R}^n$ and the function $\Phi(\mathbf{u}; \mathbf{Y}_s, t-s)$ is the dChF of the underlying dynamics given in equation (9).

So, the discounted moments of AD processes of any order can be expressed in closed form, i.e. we have all discounted moments corresponding to the monomial basis presented in Table 1. For the HHW process, of course, we base them on the H1HW approximate model.

4.2 A Bundling Method

We introduce a technique for making bundles in SGBM such that there is an equal number of paths within each bundle. It is called the *equal-number bundling* technique. The same technique of clustering paths is found in [10, 26]. The advantages of this bundling technique are that the number of paths within each bundle will grow in portion to the number of paths, and that there will be a sufficient number of paths for regression when the total number of paths is large.

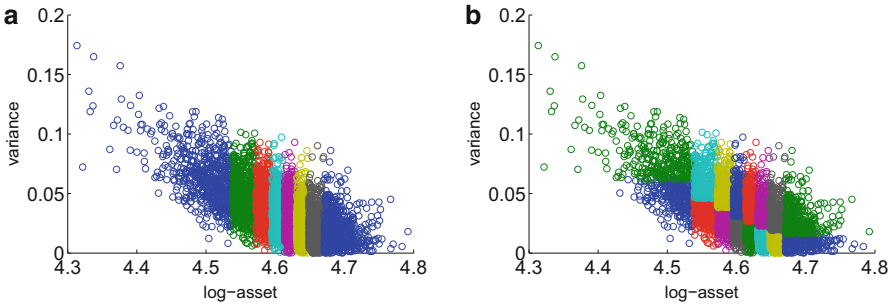

Fig. 1 Equal-number bundling. Each colored block represents a disjoint subdomain $\mathbf{I}_{m,j}$. (**a**) First iteration, J_1. (**b**) Second iteration, J_2

We use the Heston model to present the bundling technique, where the 2D state vector is denoted by $\mathbf{Y}_t = [x_t, v_t]^T$. First, all paths are sorted w.r.t. their log-asset values, and clustered into J_1 bundles with respect to their ranking, ensuring that within each bundle, the number of paths is equal to $\frac{N}{J_1}$; subsequently, within each bundle we perform a second sorting w.r.t. the variance values and cluster the paths into J_2 bundles. After these two iterations, the total number of bundles will be $J = J_1 \cdot J_2$.

The two steps are visualized in Fig. 1, where scatter plots demonstrate the 2D domain for the Heston model, at some time instant t_m. In plot (a), the paths are first clustered into 8 bundles w.r.t. the values of the log-asset, while in plot (b), the paths within each bundle are again clustered into 2 bundles w.r.t. the value of the variance. The total number of bundles is thus 16.

In a similar way, paths simulated under the HHW model can be clustered by the realized values of the log-asset (x_t), variance (v_t) and interest rate (r_t) values, in this order. We denote the number of bundles in these three dimension by J_1, J_2 and J_3, and the total number of bundles $J = J_1 \cdot J_2 \cdot J_3$.

There are other bundling approaches such as the *recursive-bifurcation-method* and the *k-means clustering method*, used in [20]. For our specific multi-dimensional problems, however, using the recursive-bifurcation-method will give rise to too few paths within some bundles when the correlation parameter ρ is close to 1 or -1, no matter how large the total number of paths is. This problem will not occur if we use the equal-number bundling technique. In addition, it is easy to implement and fast for computation compared to the k-means clustering method.

5 Numerical Tests

In this section, we will analyze the convergence and accuracy of SGBM for the Heston and the HHW models, respectively w.r.t. the following quantities:

- the value of the option at time $t = 0$;
- the EE and PFE quantities over time $[0, T]$;
- the sensitivities w.r.t. S_0 of the EE function over time $[0, T]$.

The convergence of SGBM for the computation of Bermudan options can be checked by comparing the direct and path estimators. The reference values for European and barrier options can be computed by averaging discounted cash flows for a very large number of paths.

In addition, the COS method can be connected to the MC method [31] for reference values. Under the Heston model, the COS method in [14] can be used to calculate option values and corresponding Greeks at time $t = 0$ for Bermudan and barrier options. By the MC COS method exposure profiles, quantities and sensitivities of the EE function can be computed at monitoring date t_m. We use quantities computed by the COS method as the reference values for EE, PFE and sensitivity functions under the Heston model.[2]

The Quadratic Exponential (QE) scheme is employed for accurate simulation of the Heston volatility model [1]. CVA is computed here via formula (4) with LGD = 1. The survival probability function defined in (2) is assumed to the independent of exposure with a constant intensity $h_t = 0.03$ in the period $[0, T]$.

5.1 The Heston Model

The parameters for the Heston model in (14) are chosen as

Test A: $S_0 = 100$, $r = 0.04$, $K = 100$, $T = 1$; $\kappa = 1.15$, $\gamma = 0.39$, $\bar{v} = 0.0348$, $v_0 = 0.0348$, $\rho_{x,v} = -0.64$, where the Feller condition is not satisfied.

We choose a large number of MC paths, $N = 2 \cdot 10^6$ and a relatively small time step size $\Delta t = 0.05$. The paths will be clustered into $J_1 = 2^j, J_2 = 2^j, j = 1, 2, 3, 4$ bundles. The monomial basis in SGBM is of order $p = \{1, 2, 3\}$. The number of paths is chosen large as we wish to compare the convergence and accuracy using the same set of simulated scenarios for different choices of the number of bundles J and degree p. The number of paths can be greatly reduced in real-life CVA computations because SGBM typically exhibits low variances compared to LSM.

We consider a Bermudan put option under the Heston model with parameter Test A, with 10 equally-spaced exercise dates till $T = 1$.

Figure 2a shows that the direct and path estimators converge to the option value when increasing the number of bundles (J) and the order of the monomial basis (p), as expected. Monomial basis $p = 3$ enhances the convergence speed compared to

[2] In the MC COS method, we use 400 Fourier terms, and 400 grid points in volatility direction; the COS parameter for the integration domain size is set to $L = 12$ for calculating the reference values.

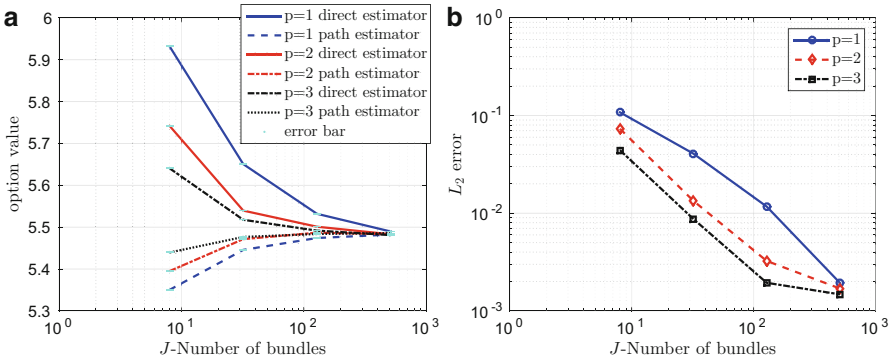

Fig. 2 Convergence of the Bermudan option value and the EE w.r.t. J—the number of bundles and p—the order of the basis functions, by comparing the direct and path estimators. Strike $K = 100$, expiry date $T = 1$ and exercise times 10. The total number of paths $N = 2 \cdot 10^6$. (**a**) Bermudan option. (**b**) Error in EE

$p = 2$ or $p = 1$. Figure 2b confirms this by showing the difference in the computed EE of the direct and path estimators, where the difference is measured in the relative L_2 norm.[3]

In Fig. 3, we present the accuracy of SGBM for the exposure quantities, EE, PFE and sensitivities of EE, by comparing to reference values by the MC COS method based on the same set of MC paths. Increasing the number of bundles J and/or the order of the monomial basis p enhances the accuracy of the results, as expected. In particular, a basis of order $p = 2$ achieves the same level of accuracy as order $p = 3$ with twice more bundles. By increasing the number of bundles, we can thus employ a monomial basis of lower order, which is an important insight.

Table 2 presents option values as well as CVA and sensitivities computed by SGBM plus the corresponding reference values. We see that the direct estimators have smaller variances compared to the path estimators.

In addition, Fig. 4 demonstrates the convergence of SGBM based on basis functions of lower order, $p = 1$, where we increase the number of bundles to 4^6. The conclusion in Appendix 4, i.e. when the size of a bundle approaches zero, the bias caused by approximating a continuous function by a simple linear function goes to zero, is confirmed. This is one advantage of SGBM compared to LSM. We need fewer basis functions by using bundles.

[3]The relative L_2 norm is defined by:

$$\frac{\|EE_{direct} - EE_{path}\|_2}{\|EE_{direct}\|_2} = \frac{\sqrt{\sum_{m=0}^{M} \left(\mathrm{EE}_{direct}(t_m) - \mathrm{EE}_{path}(t_m)\right)^2}}{\sqrt{\sum_{m=0}^{M} \left(\mathrm{EE}_{direct}(t_m)\right)^2}}. \tag{55}$$

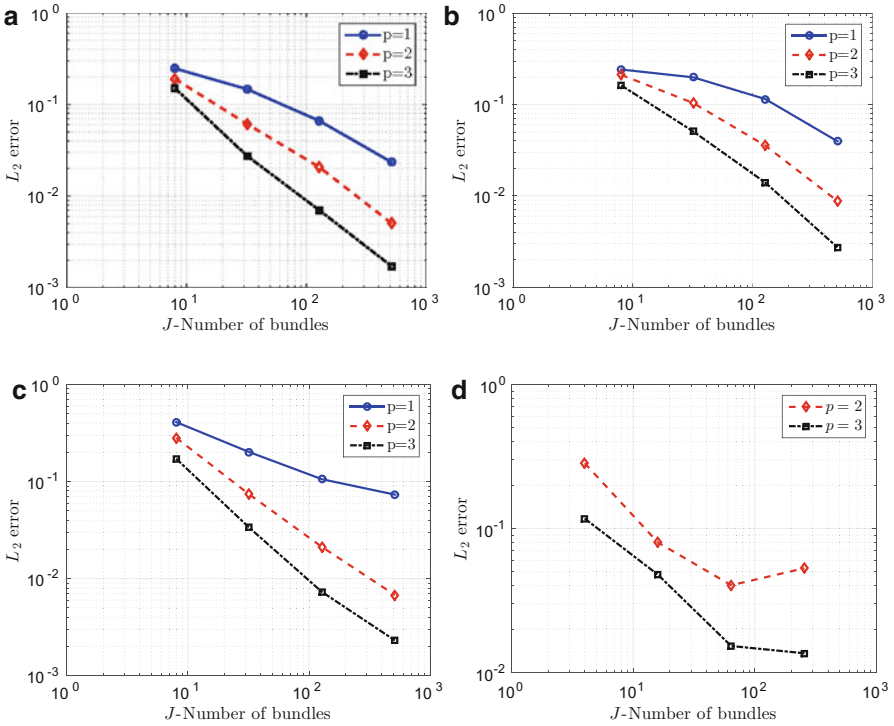

Fig. 3 Convergence of the EE, PFE and sensitivities, w.r.t. J—the number of bundles and p—the order of basis functions for a Bermudan put option; the reference is generated by the MC COS method. Strike $K = 100$, expiry date $T = 1$ and exercise times 10. The total number of paths $N = 2 \cdot 10^6$. (**a**) Error in EE. (**b**) Error in PFE. (**c**) Error in Δ_{EE}. (**d**) Error in Γ_{EE}

Table 2 Results of a Bermudan put option under the Heston model. Strike $K = 100$, expiry date $T = 1$ and exercise times 10. The total number of paths $N = 2 \cdot 10^6$, and the order $p = 2$ and the bundle number $J = 2^8$

Bermudan option under the Heston model			
Quantities	Direct estimator (std.)	Path estimator (std.)	COS
$V(0)$	5.486(0.000)	5.488 (0.005)	5.486
$\Delta_{\text{EE}}(0)$	−0.329(0.000)	–	−0.328
$\Gamma_{\text{EE}}(0)$	0.022(0.000)	–	0.025
CVA	0.093(0.000)	0.093 (0.000)	0.093 (0.000)

We also consider a put-down-out barrier option with strike $K = 100$. The option is knocked out when the asset value reaches barrier level $H = 0.9K$ before the maturity $T = 1$. After being knocked out, an investor receives a rebate value, $r_b = 10$; otherwise the investor receives the payoff at time $T = 1$. We present these quantities computed by SGBM and the corresponding reference values in Table 3.

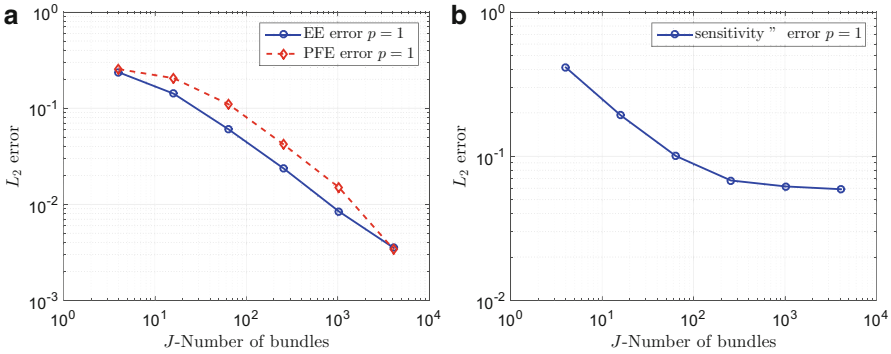

Fig. 4 Convergence of the EE, PFE and sensitivity Δ w.r.t. J—the number of bundles for a Bermudan put option when the number of paths within each bundle is 200, the order of the basis functions $p = 1$, and the total number of paths is $200J$; the reference is generated by the MC COS method . (**a**) EE and PFE when $p = 1$. (**b**) Sensitivity Δ when $p = 1$

Table 3 Results of a down-and-out barrier put option under the Heston model. Strike $K = 100$, expiry date $T = 1$, barrier level $H = 0.9K$, $r_b = 10$. The total number of paths $N = 2 \cdot 10^6$, and the order $p = 2$ and the bundle number $J = 2^8$

Barrier option under the Heston model			
Values $t = 0$	SGBM (std.)	Monte Carlo (std.)	COS
$V(0)$	4.013 (0.000)	4.016 (0.003)	4.015
$\Delta_{\text{EE}}(0)$	−0.2631 (0.000)	–	−0.263
$\Gamma_{\text{EE}}(0)$	0.0232 (0.000)	–	0.0224
CVA	0.0493 (0.000)	0.0493 (0.000)	0.0493 (0.000)

5.2 *The HHW Model*

SGBM for the Heston Hull-White model is based on forward simulation under the true HHW dynamics while the backward computation employs the discounted moments of the H1HW dynamics.There are basically two issues regarding the SGBM computation of exposure under the HHW model. We will focus on the impact of a long expiry date (say $T = 10$), and we will examine the accuracy of the approximation of the HHW model by the affine H1HW model.

We use the following parameters for the HHW and H1HW models (14):

Test B: $S_0 = 100$, $v_0 = 0.05$, $r_0 = 0.02$; $\kappa = 0.3$, $\gamma = 0.6$, $\bar{v} = 0.05$, $\lambda = 0.01$, $\eta = 0.01$, $\theta = 0.02$, $\rho_{x,v} = -0.3$ and $\rho_{x,r} = 0.6$. $T = 10$.

Simulation is done with $N = 10^6$ MC paths and $\Delta t = 0.1$. The details of the SGBM algorithm are as follows: the number of bundles varies as $J_1 = 2^{2+j}$, $J_2 = 2^j$, $J_3 = 2^j$, $j = 1, 2, 3$ and the orders of the monomial basis are $p = \{1, 2\}$.

Table 4 Implied volatility (%) obtained for a European put option with expiry date $T = 10$ under the HHW model, based on 5 simulations

Implied volatility (%)			
K/S_0	SGBM (std.)	Monte Carlo (std.)	Abs. error (%)
40%	26.481 (0.003)	26.479 (0.03)	0.0014
80%	20.699 (0.003)	20.719 (0.02)	0.0202
100%	19.200 (0.003)	19.242 (0.01)	0.0413
120%	18.369 (0.003)	18.427 (0.01)	0.0585
180%	18.220 (0.003)	18.291 (0.02)	0.0706

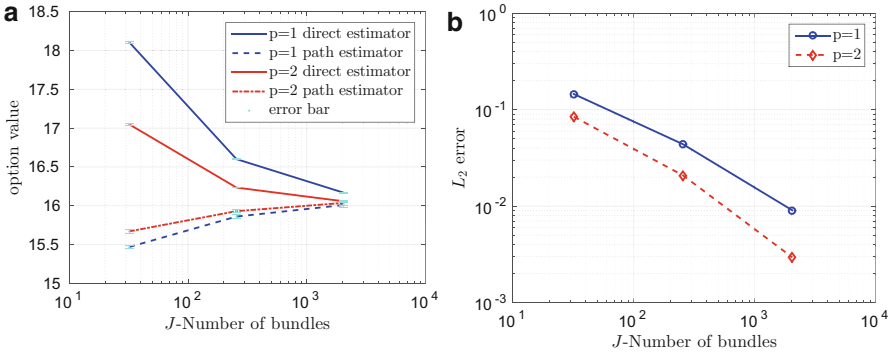

Fig. 5 Convergence w.r.t. J—the number of bundles and p—the order of the monomial basis by comparing the path and the direct estimator under the HHW model. Strike $K = 100$, $T = 10$ and 50 exercise times. The total number of paths $N = 10^6$. (**a**) Bermudan option values. (**b**) EE difference

The accuracy of SGBM is first studied by computing a European put option with $T = 10$. The implied volatility (in %) is used to demonstrate the accuracy of the computed option values, as the implied volatility is typically sensitive to the accuracy of option values [17]. The implied volatility is computed by means of the BS formula for strike values $K = \{40, 80, 100, 120, 180\}$. The reference values are computed by the average cash flows on the generated MC paths. The results are presented in Table 4. The SGBM results have smaller variances compared to results of a plain Monte Carlo simulation, and maintain a high accuracy when comparing the absolute errors.

We then consider a Bermudan put option with 50 exercise dates equally distributed in the period $[0, T]$. Figure 5 shows the SGBM convergence rate by comparing the direct and path estimators. Results of this Bermudan put are presented in Table 5. Table 6 presents results of SGBM for computing a down-and-out barrier put option. It shows that SGBM works well also for a non-continuous payoff function.

Table 5 Results for a Bermudan put option under the HHW model. Strike $K = 100$, $T = 10$ and 50 exercise times. The total number of paths is $N = 10^6$, and the order $p = 2$ and bundle number $J = 2048$

Bermudan option under the HHW model			
$T = 10$	Values $t = 0$	Direct estimator (std.)	Path estimator (std.)
	$V(0)$	16.056(0.002)	16.009 (0.018)
	$\Delta_{\text{EE}}(0)$	−0.268(0.000)	–
	$\Gamma_{\text{EE}}(0)$	0.815(0.001)	–
	CVA	2.968(0.003)	–

Table 6 Results for a down-and-out barrier put option under the HHW model. Strike $K = 100$, $T = 10$, barrier level $H = 0.9K$, $r_b = 0$. The total number of paths is $N = 10^6$, and the order $p = 2$ and $J = 2048$ bundles

Barrier option under the HHW model		
Values $t = 0$	Direct estimator (std.)	Monte Carlo (std.)
$V(0)$	0.0478(0.000)	0.0477 (0.001)
$\Delta_{\text{EE}}(0)$	0.0017(0.000)	–
$\Gamma_{\text{EE}}(0)$	−0.0001(0.000)	–
CVA	0.0123(0.000)	–

Table 7 Calculation time in seconds for computing exposure profiles of a Bermudan option and for that of a whole portfolio with expiry date $T = 10$ under the HHW model; SGBM with polynomial order $p = 2$, number of paths $N = 10^6$ and time step size $\Delta t = 0.1$

Calculation time	Direct estimator	Path estimator for Bermudan
A single (Bermudan) option	151.5 (sec.)	130.2 (sec.)
Portfolio	306.3 (sec.)	131.5 (sec.)

5.3 Speed

One benefit of the SGBM algorithm is that one can calculate different financial derivatives on the same underlying in one backward iteration using the same set of simulated paths, as the monomial basis and the discounted moments are the same. Table 7 compares the calculation time of a single Bermudan option and of a portfolio, that consists of a Bermudan option, a European option and two barrier options with the same underlying stock. The algorithm is implemented in MATLAB, and runs on an Intel(R) Core(TM) i7-2600 CPU @ 3.40GHz.

By using parallelization of the SGBM algorithm, the speed can be further enhanced drastically, see a study in [26].

Table 8 CVA(%) of European options with $T = 5$ and strike values $K = \{80, 100, 120\}$

European option, CVA (%)					
	K/S_0	BS	Heston	BSHW	HHW
$T = 1$	80%	2.951 (0.010)	2.959 (0.003)	2.953 (0.005)	2.949 (0.005)
	100%	2.956 (0.011)	2.958 (0.003)	2.952 (0.002)	2.952 (0.002)
	120%	2.955 (0.002)	2.959 (0.001)	2.953 (0.001)	2.952 (0.001)
$T = 5$	80%	13.925 (0.036)	13.941 (0.021)	13.882 (0.016)	13.929 (0.027)
	100%	13.951 (0.039)	13.960 (0.010)	13.901 (0.003)	13.940 (0.018)
	120%	13.919 (0.010)	13.953 (0.007)	13.901 (0.005)	13.936 (0.010)

5.4 Impact of Stochastic Volatility and Stochastic Interest Rates

We here check the impact of stochastic volatility and stochastic interest rates on exposure profiles and CVA. Next to the already discussed Heston and HHW models, we also consider the Black-Scholes (BS) and the Black-Scholes Hull-White (BSHW) models in this section. The parameter set chosen is the same as in Test B. For comparison, we use the parameters of the other models such that we can ensure that the values of a European put option with a fixed expiry date T has the same price under all models.[4]

We define a so-called CVA percentage as $\left(100 \cdot \frac{\text{CVA}}{V(0)}\right)\%$. Table 8 presents the percentage CVA for European put options with two maturity times, $T = \{1, 5\}$, for the strike values $K = \{80, 100, 120\}$. It can be seen that the CVA percentage does not change with strike; furthermore, European options with maturity $T = 5$ exhibit a higher CVA percentage than those with maturity $T = 1$. Based on the chosen parameters, we see only a small impact of stochastic volatility and stochastic interest rate on the CVA percentage.

Table 9 presents the percentage CVA for Bermudan put options with maturity times $T = \{1, 5\}$ for strike values $K = \{80, 100, 120\}$. We see that the 'in-the-money' options have the smallest CVA percentage. This is understandable as the optimal exercise strategy, in this paper, does not take into account the risk of a counterparty default. A put option is likely to be exercised before maturity when the strike value is higher than the current stock value, and thus one can expect relatively little exposure.

Figure 6 presents the EE and PFE function values w.r.t. time for a Bermudan put option which is at-the-money.

[4]For example, under the Black-Scholes model, we use the implied interest rate, i.e. $r_T = -\frac{\log(p(0,T))}{T}$, and compute the implied volatility by the analytic BS formula. Under the Heston model, the parameters of the Heston process are the same as those in Test B, and the corresponding interest rate is computed by the bisection algorithm. Under the BSHW model, the parameters of the Hull White process are the same as those in Test B, and the corresponding volatility is determined.

Table 9 CVA(%) of Bermudan options with $T = 5$ and strike values $K = \{80, 100, 120\}$

Bermudan option, CVA (%)					
	K/S_0	BS	Heston	BSHW	HHW
$T = 1$	80%	2.534 (0.007)	2.460 (0.002)	2.643 (0.003)	2.504 (0.003)
	100%	2.005 (0.003)	1.939 (0.002)	2.165 (0.001)	2.016 (0.001)
	120%	0.906 (0.002)	1.031 (0.001)	0.986 (0.001)	1.068 (0.001)
$T = 5$	80%	10.110 (0.032)	9.876 (0.030)	12.612 (0.014)	10.890 (0.029)
	100%	7.784 (0.011)	8.120 (0.012)	10.965 (0.008)	9.649 (0.019)
	120%	4.453 (0.008)	4.416 (0.020)	6.923 (0.005)	6.259 (0.013)

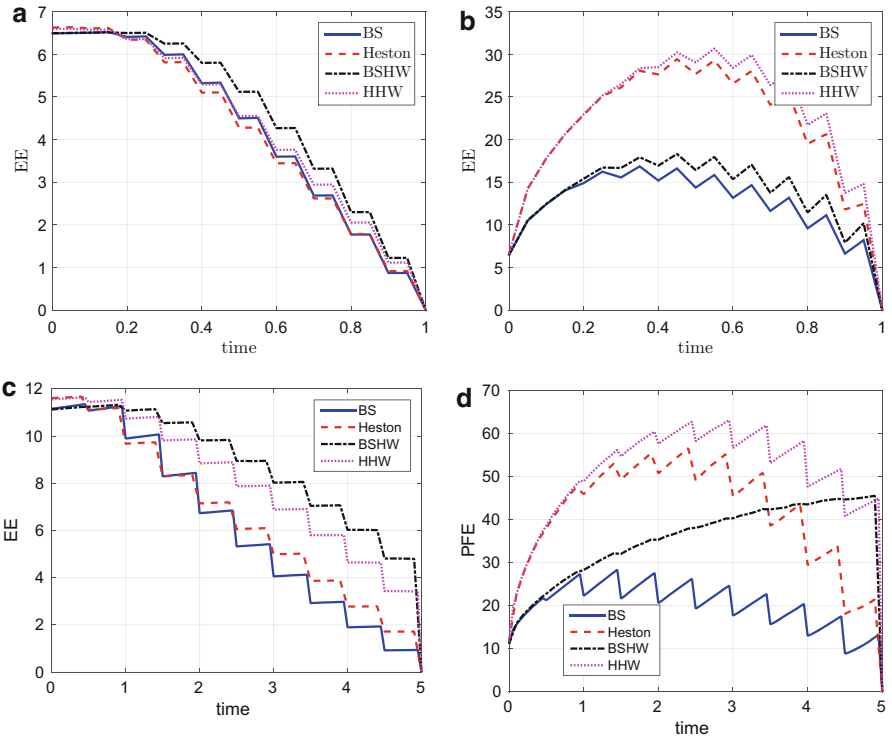

Fig. 6 Impact of stochastic volatility and interest rate on EE and PFE with different tenors and different asset dynamics, at the money $K = 100$. (**a**) T=1, EE. (**b**) T=1, PFE . (**c**) T=5, EE. (**d**) T=5, PFE

- In Fig. 6b, it can be seen that the PFE values for the HHW model are relatively close to those of the Heston model, and the PFE values for the BSHW model are very similar to those of the BS model. With a short time to maturity ($T = 1$), under our model assumptions and parameters, the stochastic volatility has a more significant contribution to the PFE values compared to the stochastic interest rate.

Compared to Fig. 6a, we can see that the EE values for the Heston and the BS models are very close. Adding stochastic volatility has more impact on the right-side tails of the exposure profiles than on the EE values.

- In Fig. 6d, in the period $t = [0, 1]$, we see similarities of PFE values between the HHW and the Heston models, and between the BS and the BSHW models; in the period $t = [1, 5]$, the PFE values for the BSHW model tend to be higher than those of the BS model, and the PFE values for the HHW model are also higher than those of the Heston model. Clearly, interest rates have more impact on the exposure profiles in the longer term (say $T = 5$).
- Figures 6a and c show that the stochastic interest rate increases the future EE values of Bermudan options, while the stochastic volatility has the opposite effect.
- The PFE curve for the BSHW model in Fig. 6d looks differently from the other curves because of the positive correlation parameter ($\rho_{x,r} = 0.6$) and the long expiry ($T = 5$). The PFE curve represents events with large option values and for a put option, this means that the associated stock values are low. In the case of a positive correlation parameter $\rho_{x,r}$, the interest rate is low as well. The investor likely holds on to the option. If we set the correlation value to zero in the BSHW model and perform the same computation, the PFE curves under the BSHW model becomes 'spiky' as well.

The stochastic interest rate plays a significant role in the case of a longer maturity derivatives, and results in increasing PFE profiles; stochastic asset volatility appears to have an effect on PFE values at the early stage of a contract. Under the parameters chosen here, at an early stage of the contract (say $t < 1$), the PFE profiles under the HHW model are very similar to those under the Heston model, but at later contract times the PFE profiles under the HHW model increase. It seems that the stochastic volatility has more effect on the right-side tail compared to the expectation of the exposure profile, while adding the stochastic interest rate increases the whole exposure profile, especially in the case of a longer maturity.

6 Conclusion

In this paper we generalize the Stochastic Grid Bundling Method (SGBM) towards the computation of exposure profiles and sensitivities for asset dynamics with stochastic asset volatility and stochastic interest rate for European, Bermudan as well as barrier options. The algorithmic structure as well as the essential method components are very similar for CVA as for the computation of early-exercise options, which makes SGBM a flexible CVA valuation framework.

We presented arguments for the choice of the basis functions for the local regression, presented a bundling technique, and showed SGBM convergence of the direct and path estimators with respect to an increasing number of bundles. Numerical experiments demonstrate SGBM's convergence and accuracy.

Using higher-order polynomials as the basis functions is especially important when accurate sensitivities values are needed; otherwise, a polynomial order $p = 1$ is sufficient for option prices and exposure quantities with a sufficiently large number of bundles and paths. The computational efficiency is connected to the number of bundles used in SGBM. A parallel algorithm will be important for a drastic reduction of the computation times, see the studies in [26].

Acknowledgements We thank Lech A. Grzelak, Shashi Jain, Kees de Graaf and Drona Kandhai for helpful discussions, as well as the CVA team at ING bank. Financial support by the Dutch Technology Foundation STW (project 12214) is gratefully acknowledged.

Appendix 1: The Joint Discounted ChF of the Heston Model

The discounted ChF of an affine model can be derived by Ricatti ODEs, as presented by Duffie et al. [13]. The expression for the joint dChF of the Heston model is given by:

$$\Phi_{\text{Heston}}(u_1, u_2, T|\mathbf{Y}_t) = \exp\left(\bar{A}_H(u_1, u_2, \tau) + \bar{B}_H(u_1, \tau)x_t + \bar{C}_H(u_1, u_2, \tau)v_t\right), \quad (56)$$

where the coefficients of the ChF are obtained via the following ODEs:

$$\frac{d\bar{B}_H}{d\tau}(u_1, \tau) = 0, \quad (57)$$

$$\frac{d\bar{C}_H}{d\tau}(u_1, u_2, \tau) = \bar{B}_H(\tau)(\bar{B}_H(\tau) - 1)/2 \quad (58)$$

$$+ \left(\gamma\rho_{x,v}\bar{B}_H(\tau) - \kappa\right)\bar{C}_H(\tau) + \gamma^2\bar{C}_H^2(\tau)/2, \quad (59)$$

$$\frac{d\bar{A}_H}{d\tau}(u_1, u_2, \tau) = \kappa\bar{v}\bar{C}_H(\tau) + r(\bar{B}_H(\tau) - 1), \quad (60)$$

where $\tau = T - t$ and initial condition $\bar{B}_H(u_1, \tau = 0) = iu_1$, $\bar{C}_H(u_1, u_2, \tau = 0) = iu_2$ and $\bar{A}_H(u_1, u_2, \tau = 0) = 0$. The solution is given by:

$$\bar{B}_H(u_1, \tau) = iu_1, \quad (61)$$

$$\bar{C}_H(u_1, u_2, \tau) = r_+ - \frac{2D_1}{\gamma^2\left(1 - ge^{-D_1\tau}\right)}, \quad (62)$$

$$\bar{A}_H(u_1, u_2, \tau) = I_1^H + I_2^H, \quad (63)$$

with

$$g = \frac{iu_2 - r_-}{iu_2 - r_+}, D_1 = \sqrt{(\kappa - \gamma\rho_{x,v}iu_1)^2 + \gamma^2 u_1(u_1 + i)}, \quad (64)$$

$$r_{\pm} = \frac{1}{\gamma^2}\left(\kappa - \gamma\rho_{x,v} i u_1 \pm D_1\right), \tag{65}$$

and

$$I_1^H = \kappa\bar{v}\left(r_- \tau - \frac{2}{\gamma^2}\log\left(\frac{1-ge^{-D_1\tau}}{1-g}\right)\right), \tag{66}$$

$$I_2^H = r(iu_1 - 1)\tau. \tag{67}$$

The form of the characteristic function in Heston's original paper [18] is problematic due to branch cuts. A more recent reference is [15]. We use the correct form of the characteristic function in our numerical examples.

Appendix 2: The Joint Discounted ChF of the Black-Scholes Hull-White Model

The expression for the joint dChF for the BSHW model is given by:

$$\Phi_{\text{BSHW}}(u_1, u_3, T|\mathbf{Y}_t) = \exp\left(\bar{A}_S(u_1, u_3, \tau) + \bar{B}_S(u_1, \tau)x_t + \bar{D}_S(u_1, u_3, \tau)r_t\right), \tag{68}$$

where the coefficients of the ChF are obtained via the following ODEs:

$$\frac{d\bar{B}_S}{d\tau}(u_1, \tau) = 0, \tag{69}$$

$$\frac{d\bar{D}_S}{d\tau}(u_1, u_3, \tau) = -1 + \bar{B}_S(u_1, \tau) - \lambda\bar{D}_S(u_1, u_3, \tau), \tag{70}$$

$$\begin{aligned}\frac{d\bar{A}_S}{d\tau}(u_1, u_3, \tau) = {} & \frac{1}{\sigma^2}\bar{B}_S(u_1, \tau)\left(\bar{B}_S(u_1, \tau) - 1\right) + \lambda\cdot\theta(T-\tau)\cdot\bar{D}_S(u_1, u_3, \tau) \\ & + \frac{1}{2}\eta^2\bar{D}_S(u_1, u_3, \tau) + \rho_{x,r}\sigma\eta\bar{B}_S(u_1, \tau)\bar{D}_S(u_1, u_3, \tau),\end{aligned} \tag{71}$$

where $\tau = T - t$ and initial condition $\bar{B}_S(u_1, \tau = 0) = iu_1$, $\bar{D}_S(u_1, u_3, \tau = 0) = iu_3$, and $\bar{A}_S(u_1, u_3, \tau = 0) = 0$. The solution is now given by:

$$\bar{B}_S(u_1, \tau) = iu_1, \tag{72}$$

$$\bar{D}_S(u_1, u_3, \tau) = \frac{iu_1 - 1}{\lambda}\left(1 - e^{-\lambda\tau}\right) + iu_3 e^{-\lambda\tau}, \tag{73}$$

$$\bar{A}_S(u_1, u_3, \tau) = I_1^S + I_2^S + I_3^S + I_4^S, \tag{74}$$

with

$$I_1^S = \frac{1}{2}\sigma^2 i u_1 (i u_1 - 1)\tau, \tag{75}$$

$$I_2^S = \int_0^\tau \theta(T-s)\cdot \bar{D}_S(u_1, u_3, s) ds \tag{76}$$

$$I_3^S = \frac{\eta^2}{2\lambda^2}\Bigg(\frac{2}{\lambda}(u_1+i)(e^{-\lambda\tau}-1)(\lambda u_3 - u_1 - i) + \frac{1}{2\lambda}\left(e^{-2\lambda\tau}-1\right)(\lambda u_3 - u_1 - i)^2 - (u_1+i)^2\tau\Bigg), \tag{77}$$

$$I_4^S = \frac{\eta\theta\sigma\rho_{x,r}}{\lambda}\left(-\frac{i u_1 + u_1^2}{\lambda}(\lambda\tau + e^{-\lambda\tau} - 1) + u_1 u_3 (e^{-\lambda\tau}-1)\right). \tag{78}$$

When $\theta(t) = \theta$ is a constant,

$$I_2^S = \theta\left((i u_1 - 1)\tau + \frac{1}{\lambda}(e^{-\lambda\tau}-1)(i u_1 - 1) - i u_3\left(e^{-\lambda\tau}-1\right)\right). \tag{79}$$

Again the discounted moments are obtained by symbolic computations in MATLAB.

Appendix 3: The Joint Discounted ChF of the H1HW Model

The expression for the joint dChF of the H1HW model is given by:

$$\Phi_{\text{H1HW}}(u_1, u_2, u_3, T|\mathbf{Y}_t) = \exp\left(\bar{A}_W(u_1, u_2, u_3, \tau) + \bar{B}_W(u_1, \tau)x_t + \bar{C}_W(u_1, u_2, \tau)v_t + \bar{D}_W(u_1, u_3, \tau)r_t\right), \tag{80}$$

where the coefficients of the ChF are here obtained via the following ODEs:

$$\frac{d\bar{B}_W}{d\tau}(u_1, \tau) = 0, \tag{81}$$

$$\frac{d\bar{C}_W}{d\tau}(u_1, u_2, \tau) = \bar{B}_W(\tau)(\bar{B}_W(\tau)-1)/2 + \left(\gamma\rho_{x,v}\bar{B}_W(\tau) - \kappa\right)\bar{C}_W(\tau) + \gamma^2\bar{C}_W^2(\tau)/2, \tag{82}$$

$$\frac{d\bar{D}_W}{d\tau}(u_1, u_3, \tau) = -1 + \bar{B}_W(u_1, \tau) - \lambda\bar{D}_W(u_1, u_3, \tau), \tag{83}$$

$$\frac{d\bar{A}_W}{d\tau}(u_1, u_2, u_3, \tau) = \lambda\cdot\theta(T-\tau)\cdot\bar{D}_W(u_1, u_3, \tau) + \kappa\bar{v}\bar{C}_W(u_1, u_2, \tau)$$

$$+\frac{1}{2}\eta^2\bar{D}_W^2(u_1,u_3)+\eta\rho_{x,v}\mathbb{E}\left[\sqrt{v_T}\middle|v_t\right]\bar{B}_W(u_1,\tau)\bar{D}_W \times(u_1,u_3,\tau), \tag{84}$$

where $\tau = T-t$ and initial condition $\bar{B}_W(u_1,\tau=0)=iu_1$, $\bar{C}_W(u_1,u_2,\tau=0)=iu_2$, $\bar{D}_W(u_1,u_3,\tau=0)=iu_3$ and $\bar{A}_W(u_1,u_2,u_3,\tau=0)=0$. The solution is given by:

$$\bar{B}_W(u_1,\tau) = iu_1, \tag{85}$$

$$\bar{C}_W(u_1,u_2,\tau) = r_+ - \frac{2D_1}{\gamma^2\left(1-ge^{-D_1\tau}\right)}, \tag{86}$$

$$\bar{D}_W(u_1,u_3,\tau) = \frac{iu_1-1}{\lambda}\left(1-e^{-\lambda\tau}\right)+iu_3e^{-\lambda\tau}, \tag{87}$$

$$\bar{A}_W(u_1,u_2,u_3,\tau) = I_1^W+I_2^W+I_3^W+I_4^W, \tag{88}$$

where expressions g, D_1 and $r_\pm$ are the same as in (64), and

$$I_1^W = \int_0^\tau \theta(T-s)\cdot\bar{D}_W(u_1,u_3,s)ds, \tag{89}$$

$$I_2^W = \kappa\bar{v}\left(r_-\tau-\frac{2}{\gamma^2}\log\left(\frac{1-ge^{-D_1\tau}}{1-g}\right)\right), \tag{90}$$

$$I_3^W = \frac{\eta^2}{2\lambda^2}\left(\frac{2}{\lambda}(u_1+i)(e^{-\lambda\tau}-1)(\lambda u_3-u_1-i)\right. \tag{91}$$

$$\left.+\frac{1}{2\lambda}\left(e^{-2\lambda\tau}-1\right)(\lambda u_3-u_1-i)^2-(u_1+i)^2\tau\right), \tag{92}$$

$$I_4^W = \eta\rho_{x,r}\left(-\frac{iu_1+u_1^2}{\lambda}G_1(\tau,v_t)-u_1u_3G_2(\tau,v_t)\right), \tag{93}$$

where

$$G_1(\tau,v_t) := \int_0^\tau \mathbb{E}\left[\sqrt{v_{T-x}}\middle|v_t\right]\left(1-e^{-\lambda x}\right)dx, \tag{94}$$

$$G_2(\tau,v_t) := \int_0^\tau \mathbb{E}\left[\sqrt{v_{T-x}}\middle|v_t\right]e^{-\lambda x}dx. \tag{95}$$

When $\theta(t)=\theta$ is a constant, I_1 can be integrated by

$$I_1^W = \theta\left((iu_1-1)\tau+\frac{1}{\lambda}(e^{-\lambda\tau}-1)(iu_1-1)-iu_3\left(e^{-\lambda\tau}-1\right)\right). \tag{96}$$

It is computationally expensive to calculate the integral for G_1 and G_2 over $[t, t+\tau]$. We use an approximation where, for a fixed v_t, values of the conditional expectation $\mathbb{E}\left[\sqrt{v_{t+\tau}}\middle| v_t\right]$ over a short time period can be approximated by a linear function w.r.t. time.

We will use the approximation that

$$\mathbb{E}\left[\sqrt{v_{t+\tau}}\middle| v_t\right] \approx a(v_t) + b(v_t, \Delta t)\tau, \quad \tau \leq \Delta t, \tag{97}$$

where $a(v_t) = \sqrt{v_t}$, $b(v_t, \Delta t) = \frac{v_{(t+\Delta t)} - v_t}{\Delta t}$, $\Delta t = 0.05$. Various experiments have shown that this approximation is sufficiently accurate in the present context.

The integrals expressed in (94) and (95) can be approximated by an analytic formula with the approximation in (97). To further enhance the of SGBM, we compute the integrals on a volatility grid based on the minimum and maximum values of the variance on the simulated paths. At each time step t_m, the discounted moments on all paths are computed with the help of the volatility grid plus a spline interpolation technique.

Appendix 4: Errors of Approximation of the Option Function

There are two types of errors when approximating the option function on the bounded domain $\mathbf{U}^j_{m+1}$ at time t_{m+1}. The first type of error ϵ_1 is the difference between the real option function and its projection on the polynomial space $\mathscr{P}(\mathbf{U}^j_{m+1}, p)$, and the second type of error ϵ_2 is the difference between the real projection on the polynomial space and its statistical approximation given a data set $\{\hat{v}_{m+1}(i), \hat{\mathbf{y}}_{m+1}(i)\}$. Measured in L_2 norm within the j-bundle, these two errors can be expressed by

$$\epsilon_1 = \|V(t_{m+1}, \cdot) - Z_1(t_{m+1}, \cdot)\|_{L_2}, \tag{98}$$

$$\epsilon_2 = \|Z_1(t_{m+1}, \cdot) - Z_2(t_{m+1}, \cdot)\|_{L_2}. \tag{99}$$

where the L_2 norm is defined by the conditional probability measure $\mu_{(\mathbf{Y}_{m+1}|\mathbf{Y}_m)}$, i.e. for any L_2 measurable function $f(\mathbf{Y}_{m+1})$, its L_2 norm is defined by [29]

$$\|f\|_{L_2} = \left(\int_{\mathbf{Y}_{m+1}\in\mathbb{R}^n} |f(\mathbf{Y}_{m+1})|^2 d\mu_{(\mathbf{Y}_{m+1}|\mathbf{Y}_m)}\right)^{\frac{1}{2}}. \tag{100}$$

It is trivial to see that the total error of approximation of the option function is bounded by the sum of these two types of error, i.e.

$$\mathbb{E}^{\mathbb{Q}}\left[\left(V(t_{m+1}, \mathbf{Y}_{m+1}) - Z_2(V(t_{m+1}, \mathbf{Y}_{m+1})\right)^2 \middle| \mathbf{Y}_m\right] \leq \epsilon_1 + \epsilon_2, \tag{101}$$

and we will discuss them respectively.

- For the first type of error ϵ_1: The well-known Weierstrass approximation theorem states that any continuous function defined on a closed interval can be uniformly approximated as closely as desired by a polynomial function [24]. It can ensure that ϵ_1 will go to zero as the order of the monomial basis goes to infinity.
  More specifically, the error ϵ_1 is involved with the property of the polynomial space $\mathscr{P}(\mathbf{U}_{m+1}^j, p)$, i.e. the size of the domain $\mathbf{U}_{m+1}^j$ and the order of the monomial basis p. Theorems 1.2 in [24, p.12] and Theorem 3.2 in [24, p.59] provides a priori error estimate in L_2 norm when the function needs to be approximated is twice differentiable.
  To reduce error ϵ_1, we can either reduce the size of the domain $\mathbf{U}_{m+1}^j$ or increase the order of the basis functions. By using bundles we can achieve the former goal.
- For the second type of error ϵ_2: Assuming that the function Z_2 is an unbiased statistical estimator of Z_1, i.e.

$$Z_1(t_{m+1}, \mathbf{Y}_{m+1}) = Z_2(t_{m+1}, \mathbf{Y}_{m+1}) + \delta_{m+1}, \tag{102}$$

  where the error term $\delta_{m+1} \sim \mathcal{N}(0, \sigma_{m+1}^2)$ i.i.d, where σ_{m+1}^2 is the constant variance. By central limit theorem the error satisfies with probability 1 that $\epsilon_2 \to \frac{\sigma_{m+1}}{\sqrt{N_j}}$, as the number of paths $N_j \to \infty$. It implies that the error ϵ_2 approaches zero as the number of paths goes to infinity with probability 1. Error ϵ_2 can be reduced by increasing the number of paths N_j.

As a conclusion, the SGBM approach converges as the number of bundles, the number of paths within each bundle and the polynomial order p of the basis functions go to infinity.

Appendix 5: Proof of Proposition 1

Proof By Jensen's inequality:

$$\begin{aligned}
&\Big(c(t_m, \mathbf{Y}_m) - c_2(t_m, \mathbf{Y}_m)\Big)^2 \\
&= \left(\mathbb{E}^{\mathbb{Q}}\left[D(t_m, t_{m+1})V(t_{m+1}, \mathbf{Y}_{m+1})\middle|\mathbf{Y}_m\right] - \mathbb{E}^{\mathbb{Q}}\left[D(t_m, t_{m+1})Z_2(t_{m+1}, \mathbf{Y}_{m+1})\middle|\mathbf{Y}_m\right]\right)^2 \\
&\leq \mathbb{E}^{\mathbb{Q}}\left[\left(D(t_m, t_{m+1})(V(t_{m+1}, \mathbf{Y}_{m+1}) - Z_2(t_{m+1}, \mathbf{Y}_{m+1}))\right)^2 \middle|\mathbf{Y}_m\right] \\
&\leq \mathbb{E}^{\mathbb{Q}}\left[\left(V(t_{m+1}, \mathbf{Y}_{m+1}) - Z_2(t_{m+1}, \mathbf{Y}_{m+1})\right)^2 \middle|\mathbf{Y}_m\right].
\end{aligned} \tag{103}$$

References

1. L. B. G. Andersen. Simple and Efficient Simulation of the Heston Stochastic Volatility Model. *Journal of Computational Finance*, 11:1–48, 2008.
2. Bank for International Settlements. Basel II: International Convergence of Capital Measurement and Capital Standards: A Revised Framework. Technical report, 2004.
3. T. R. Bielecki and M. Rutkowski. *Credit risk: Modeling, Valuation and Hedging*. Springer Science & Business Media, 2002.
4. F. Black and M. Scholes. The Pricing of Options and Corporate Liabilities. *Journal of Political Economy*, 81(3):pp. 637–654, 1973.
5. D. Brigo. Counterparty Risk FAQ: Credit VaR, PFE, CVA, DVA, Closeout, Netting, Collateral, Re-hypothecation, WWR, Basel, Funding, CCDS and Margin Lending. Papers 1111.1331, arXiv.org, Nov 2011.
6. D. Brigo and F. Mercurio. *Interest Rate Models-Theory and Practice: with Smile, Inflation and Credit*. Springer Science & Business Media, 2007.
7. M. Broadie and M. Cao. Improved Lower and Upper Bound Algorithms for Pricing American Options by Simulation. *Quantitative Finance*, 8(8):845–861, 2008.
8. M. Broadie, P. Glasserman, and Z. Ha. Pricing American Options by Simulation Using a Stochastic Mesh with Optimized Weights. In S. Uryasev, editor, *Probabilistic Constrained Optimization*, volume 49 of *Nonconvex Optimization and Its Applications*, pages 26–44. Springer US, 2000.
9. J. F. Carriere. Valuation of the Early-exercise Price for Options Using Simulations and Nonparametric Regression. *Insurance: mathematics and Economics*, 19(1):19–30, 1996.
10. F. Cong and C. W. Oosterlee. Pricing Bermudan Options under Merton Jump-Diffusion Asset Dynamics. *International Journal of Computer Mathematics, Forthcoming*, 2015.
11. J. C. Cox, J. E, Ingersoll, and S. A. Ross. A Theory of the Term Structure of Interest Rates. *Econometrica*, 53(2):385–407, 1985.
12. C. S. L. de Graaf, Q. Feng, D. Kandhai, and C. W. Oosterlee. Efficient Computation of Exposure Profiles for Couterparty Credit Risk. *International Journal of Theoretical and Applied Finance*, 17(04):1450024, 2014.
13. D. Duffie, J. Pan, and K. Singleton. Transform Analysis and Asset Pricing for Affine Jump-Diffusions. *Econometrica*, 68(6):1343–1376, 2000.
14. F. Fang and C. W. Oosterlee. A Fourier-Based Valuation Method for Bermudan and Barrier Options under Heston's Model. *SIAM Journal on Financial Mathematics*, 2(1):439–463, 2011.
15. J. Gatheral. *The Volatility Surface: A Practitioner's Guide*, volume 357. John Wiley & Sons, 2011.
16. J. Gregory. *Counterparty Credit Risk: The New Challenge for Global Financial Markets*. The Wiley Finance Series. John Wiley & Sons, 2010.
17. L. Grzelak and C. W. Oosterlee. On the Heston Model with Stochastic Interest Rates. *SIAM Journal on Financial Mathematics*, 2(1):255–286, 2011.
18. S. L. Heston. A Closed-Form Solution for Options with Stochastic Volatility with Applications to Bond and Currency Options. *Review of Financial Studies*, 6(2):327–343, 1993.
19. J. Hull and A. White. Pricing Interest-Rate-Derivative Securities. *Review of financial studies*, 3(4):573–592, 1990.
20. S. Jain and C. W. Oosterlee. The Stochastic Grid Bundling Method: Efficient Pricing of Bermudan Options and Their Greeks . *Applied Mathematics and Computation*, 269:412–431, 2015.
21. R. A. Jarrow and S. M. Turnbull. Pricing Derivatives on Financial Securities Subject to Credit Risk. *Journal of Finance-New York-*, 50:53–53, 1995.
22. C. Kenyon, A. D. Green, and M. Berrahoui. Which measure for pfe?. the risk appetite measure a. *The Risk Appetite Measure A.(December 15, 2015)*, 2015.
23. D. Lando. *Credit Risk Modeling: Theory and Applications: Theory and Applications*. Princeton University Press, 2009.

24. M. G. Larson and F. Bengzon. *The Finite Element Method: Theory, Implementation, and Applications*, volume 10. Springer Science & Business Media, 2013.
25. B. Lauterbach and P. Schultz. Pricing Warrants: An Empirical Study of the Black-Scholes Model and Its Alternatives. *The Journal of Finance*, 45(4):1181–1209, 1990.
26. Á. Leitao and C. W. Oosterlee. GPU Acceleration of the Stochastic Grid Bundling Method for Early-Exercise Options. *International Journal of Computer Mathematics*, pages 1–22, 2015.
27. F. Longstaff and E. Schwartz. Valuing American Options by Simulation: A Simple Least-squares Approach. *Review of Financial Studies*, 14(1):113–147, 2001.
28. D. B. Madan and H. Unal. Pricing the Risks of Default. *Review of Derivatives Research*, 2(2–3):121–160, 1998.
29. B. Øksendal. *Stochastic Differential Equations*. Springer, 2003.
30. M. Pykhtin and S. Zhu. A Guide to Modelling Counterparty Credit Risk. *GARP Risk Review*, pages 16–22, July/August 2007.
31. Y. Shen, J. van der Weide, and J. Anderluh. A Benchmark Approach of Counterparty Credit Exposure of Bermudan Option under Lévy Process: The Monte Carlo-COS Method. *Procedia Computer Science*, 18(0):1163–1171, 2013. 2013 International Conference on Computational Science.
32. L. Stentoft. Value Function Approximation or Stopping Time Approximation: A Comparison of Two Recent Numerical Methods for American Option Pricing Using Simulation and Regression. *Journal of Computational Finance*, 18:1–56, 2010.
33. J. N. Tsitsiklis and B. Van Roy. Regression Methods for Pricing Complex American-Style Options. *Trans. Neur. Netw.*, 12(4):694–703, July 2001.
34. O. Vasicek. An Equilibrium Characterization of the Term Structure. *Journal of financial economics*, 5(2):177–188, 1977.